Vanadium(v) tetra-phenolate complexes: synthesis, structural studies and ethylene homo-(co-) polymerization capability

Vanadium(V) tetra-phenolate complexes: Synthesis, structural studies and ethylene homo-(co-)polymerization capability

Carl Redshaw,[a*] Mark J. Walton,[b] Mark R.J. Elsegood,[c] Timothy J. Prior[a] and Kenji Michiue[d]

[a] *Department of Chemistry, University of Hull, Hull, HU6 7RX, U.K.*

[b] *Energy Materials Laboratory, School of Chemistry, University of East Anglia, Norwich, NR4 7TJ, U.K.*

[c] *Chemistry Department, Loughborough University, Loughborough, Leicestershire, LE11 3TU, U.K.*

[d] *Process Technology Center, Mitsui Chemicals Inc., 580-32 Nagaura, Sodegaura, Chiba 299-0265, Japan.*

Abstract: Reaction of the ligand α,α,α′,α′-tetrakis(3,5-di-*tert*-butyl-2-hydroxyphenyl)-*p*-xylene (*p*-L^1H_4) with two equivalents of $[VO(OR)_3]$ (R = *n*Pr, *t*Bu) in refluxing toluene afforded, after work-up, the complexes $\{[VO(OnPr)(THF)]_2(\mu\text{-}p\text{-}L^1)\}\cdot 2(THF)$ (**1**·2(THF)) or $\{[VO(OtBu)]_2(\mu\text{-}p\text{-}L^1)\}\cdot 2MeCN$ (**2**·2MeCN), respectively in moderate to good yield. A similar reaction using the *meta* ligand, namely α,α,α′,α′-tetrakis(3,5-di-*tert*-butyl-2-hydroxyphenyl)-*m*-xylene (*m*-L^2H_4) afforded the complex $\{[VO(OnPr)(THF)]_2(\mu\text{-}p\text{-}L^2)\}$ (**3**). Use of $[V(Np\text{-}R^1C_6H_4)(tBuO)_3]$ (R^1 = Me, CF_3) with *p*-L^1H_4 led to the isolation of the oxo-imido complexes $\{[VO(tBuO)][V(Np\text{-}R^1C_6H_4)(tBuO)](\mu\text{-}p\text{-}L^1)\}$ (R^1 = Me, **4**·CH_2Cl_2; CF_3, **5**·CH_2Cl_2), whereas use of $[V(Np\text{-}R^1C_6H_4)Cl_3]$ (R^1 = Me, CF_3) in combination with

Et_3N/*p*-L^1H_4 or *p*-L^1Na_4 afforded the diimido complexes {[V(N*p*-MeC_6H_4)(THF)Cl]$_2$(μ-*p*-L^1)}·4toluene (**6**·4toluene) or {[V(N*p*-$CF_3C_6H_4$)(THF)Cl]$_2$(μ-*p*-L^1)} (**7**). For comparative studies, the complex [(VO)(μ-O*n*Pr)L^3]$_2$ (**8**) has also been prepared via the interaction of [VO(*n*PrO)$_3$] and 2-(α-(2-hydroxy-3,5-di-*tert*-butylphenyl)benzyl)-4,6-di-*tert*-butylphenol (L^3H_2). The crystal structures of **1**·2THF, **2**·2MeCN, **3**, **4**·CH_2Cl_2, **5**·CH_2Cl_2, **6**·4toluene·thf, **7** and **8** have been determined. Complexes **1** – **3** and **5** - **8** have been screened as pre-catalysts for the polymerization of ethylene in the presence of a variety of co-catalysts (with and without a re-activator), including DMAC (dimethylaluminium chloride), DEAC (diethylaluminium chloride), EADC (ethylaluminium dichloride) and EASC (ethylaluminium sesquichloride) at various temperatures and for the co-polymerization of ethylene with propylene; results are compared *versus* the benchmark catalyst [VO(OEt)Cl_2]. In some cases, activities as high as 243,400 g/mmolV.h (30.43 Kg PE/mmolV.h.bar) were achievable, whilst it also proved possible to obtain higher molecular weight polymers (in comparable yields to the use of [VO(OEt)Cl_2]). In all cases with dimethylaluminium chloride (DMAC)/ethyltrichloroacetate (ETA) activation, the activities achieved surpassed those of the benchmark catalyst. In the case of the co-polymerization of ethylene with propylene, Complexes **1** – **3** and **5** - **8** showed comparable or higher molecular weight than [VO(OEt)Cl_2] with comparable catalytic activities or higher in the case of the imido complexes **6** and **7**.

Keywords: Vanadium; tetra-phenolate; polyethylene; ethylene/propylene copolymer; crystal structures.

Introduction: Interest in the use of group V metal complexes as potential components in new catalytic systems for the production of new polymers from α–olefins continues to attract both academic and industrial interest. [1] This is in-part driven by the need for new IP in emerging economies such as China and India. In the case of vanadium, interest is further stimulated by the ability to achieve high activities and conduct co- and ter-polymerizations. [2] Notable recent successes have been achieved, which have made use of a variety of ligand sets including phenoxyimines, mono-dentate aryloxides, β-enaminoketonato and phenoxy-phosphine/phosphineoxides. [3] In our previous work, we have observed very high activities when employing chelating phenoxide ligands, including the use of calix[*n*]arenes, as well as di-/tri-phenols. [4] With this in mind, we were keen to explore other ligand systems that were capable of simultaneously binding to more than one metal centre. A new family of tetraphenols was recently reported by Tang *et al.* [5], which have since been exploited by the group of Wu to prepare multi alkali-metal complexes capable of the ring opening polymerization (ROP) of *L*-lactide, [6] and by us to afford niobium-based complexes capable of the ROP of ε-caprolactone. [7] Herein, we describe the synthesis and molecular structures of a series of vanadyl complexes of this ligand family (shown in Scheme 1), and investigate their polymerization catalysis behavior towards ethylene and ethylene/propylene under a variety of conditions. Extremely high catalytic activities, of the order of 243,400 g/mmolV.h at 8 bar ethylene (30.43 Kg PE/mmolV.h.bar), were found to be achievable for these systems which, combined with their ability to afford reasonably high molecular weight products at high temperature, suggests that such systems could be of industrial interest. Indeed, to the best of our knowledge, these are the highest catalytic activities reported to-date for vanadium-based systems for ethylene polymerization under robust conditions. We note though that these high activities, *versus* related systems, can be ascribed to the use of the high pressures (8 bar) employed herein. For

example, the phosphine-phenoxide complex {[2,4-(tBu)$_2$-6-PPh$_2$C$_6$H$_2$O]VCl$_2$(THF)$_2$} can achieve an activity of 41.3 KgPE/mmolV.h at 1 bar. [3d] Of the other highly active vanadium systems known (see scheme 2), the coordination at the metal tends to be a combination of nitrogen (in the form of either an organimido group of an imine linkage) and oxygen (mono- or bi-dentate phenoxide ligation) or, more recently, calix[*n*]arene derived ligation. [3, 4] High molecular weight polyethylene is an attractive product given its favorable mechanical and physical properties, though there can be issues with regard to processing. [8] We note that industrially, the co-polymerization of ethylene with higher olefins has been successfully achieved by employing group IV-based constrained geometry catalysts. For example, Dow Chemicals has also utilized complexes bearing imino-enamido or pyridyl-amido ligation for ethylene/α-olefin copolymerization and polyolefin block copolymer formation. [9, 10] However, we note that only a limited number of vanadium-based systems have been reported for ethylene/propylene co-polymerization. [4b-d, 11]

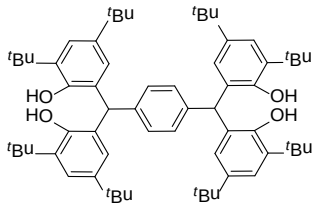

L^1H_4

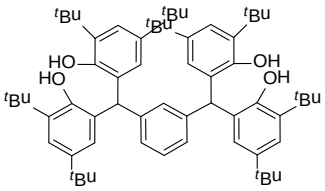

L^2H_4

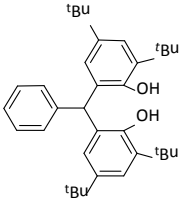

L^3H_2

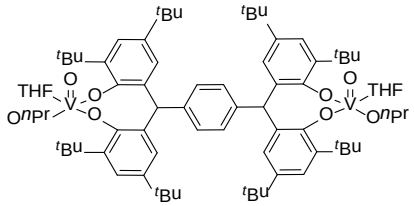

(**1**)

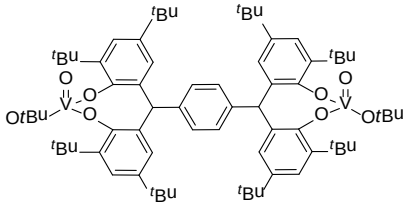

(**2**)

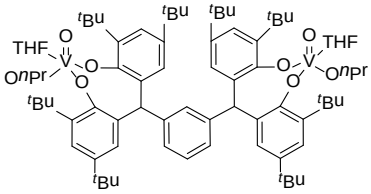

(**3**)

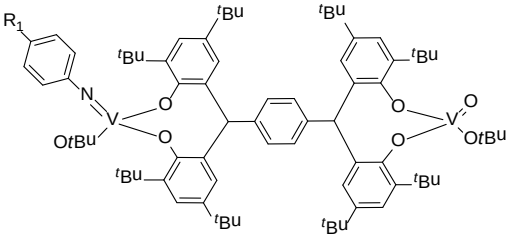

R_1 = Me (**4**), CF_3 (**5**)

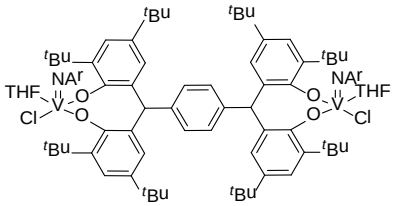

Ar = *p*-tolyl (**6**), *p*-$CF_3C_6H_4$ (**7**)

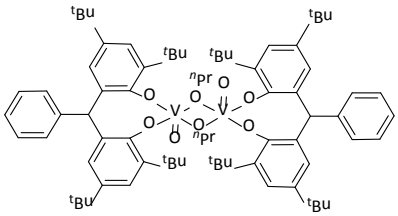

(**8**)

Scheme 1. Pre-catalysts **1** - **8** prepared herein.

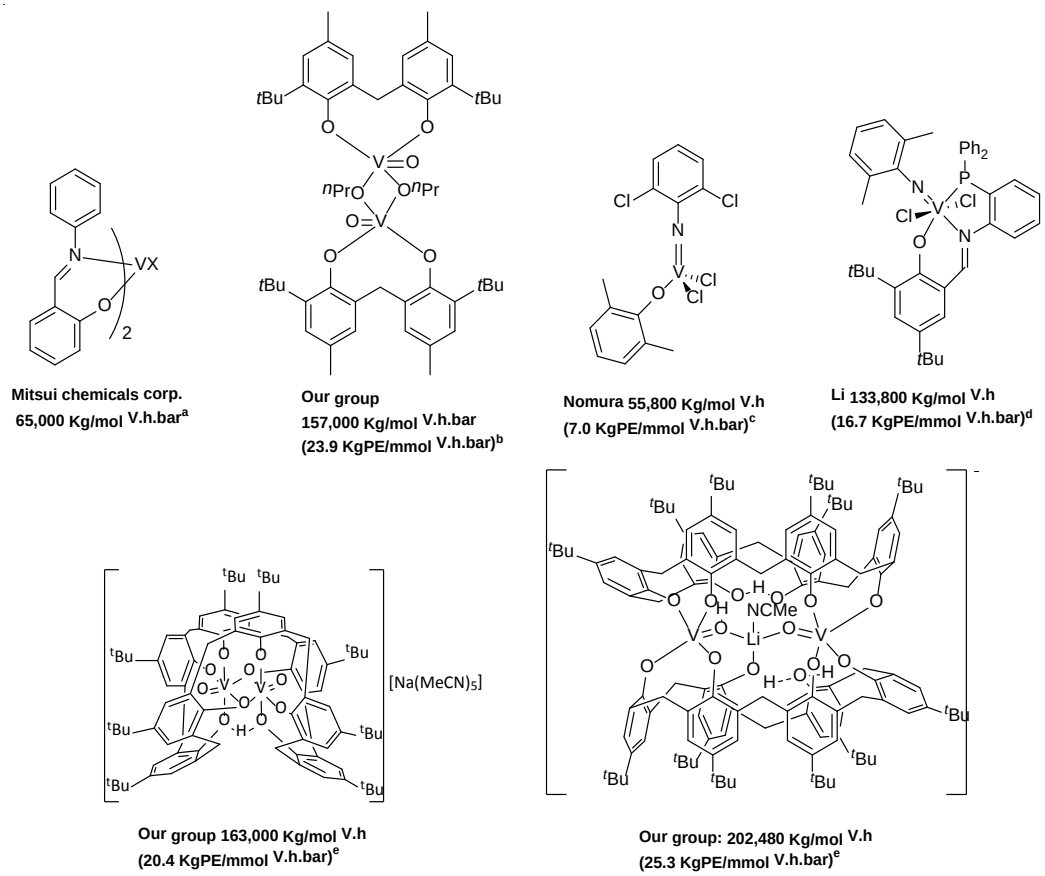

Scheme 2. Known, highly active vanadium-based ethylene polymerization pre-catalysts. [3, 4] Conditions employed: [a] [V] = 1.0 μmol, co-cat = $MgCl_2/Et_mAl(OR)_n$ (0.8 mmol Mg:2.4 mmol Et_3Al), 75 °C, 1 bar, 15 min. [b] [V] = 0.8 μmol, co-cat = Me_2AlCl (2 mmol), ETA (2 mmol), 80 °C, 7 bar, 15 min. [c] [V] = 0.05 μmol, co-cat = Et_2AlCl (2000 equiv.), 0 °C, 8 bar, 10 min. [d] [V] = 0.1 μmol, co-cat = Et_2AlCl (0.05M), 75 °C, 8 bar, 10 min. [e] [V] = 0.005 μmol, co-cat = Me_2AlCl (20000 equiv.), ETA (20000 equiv.), 80 °C, 8 bar, 30 min.

Results and Discussion

Synthesis and structure of p-L^1H_4 derived vanadyl complexes: The ligand *p*-L^1H_4 was synthesized following the reported literature method. [5] The compounds {[VO(O*n*Pr)(THF)]$_2$(μ-*p*-L^1)} (**1**) and {[VO(O*t*Bu)]$_2$(μ-*p*-L^1)} (**2**)) were synthesized in moderate to good yield (45 – 75 %) via the treatment of L^1H_4 with a slight excess (2.1 equiv.) of $[VO(OR)_3]$. If the reaction is conducted in THF, then this solvent can act as a ligand as in **1**, *vide infra*. Conducting

the reaction in toluene and avoiding the use of THF in the work-up affords THF-free products, as in **2**. In either case, the reaction proceeds with loss of two equivalents of alcohol per vanadium center. In the case of **1** (R = *n*Pr), crystals suitable for a single crystal X-ray diffraction study were grown by slow diffusion of light petroleum into THF; the crystal structure is presented in Figure 1 (for ORTEP diagram see Figure S1 in the ESI). Each vanadyl center is present in trigonal bipyramidal geometry, and bears an *n*-propoxide ligand with the fifth position *trans* to the oxo group occupied by a THF molecule. The two sets of di-phenolates across the central phenyl ring are arranged in a *trans* fashion related by an inversion center. The bond lengths and angles are given in the caption to Figure 1, and are typical and similar to the other vanadium complexes in trigonal bipyramidal geometry. [12] An 8-membered metallocycle is formed at each end of the tetra-phenolate, with each adopting the chair-boat conformation. The bite angle of the chelate is 111.73(7) ^{o}, which is somewhat larger than that found in the mononuclear vanadyl complex {VOCl[2,2$^{/}$-CH_2(4-Me-6-*t*Bu$C_6H_2O)_2$]} (106.9(2) ^{o}) and the dimeric complex {VO(O*n*Pr)(2,2$^{/}$-CH_3CH[4,6-(*t*Bu)$_2C_6H_2)_2$]} (94.49(10) ^{o}). [4, 13] In the IR spectra for **1** and **2**, a strong band at *ca*. 990 cm^{-1} is assigned to the *v*(V=O) mode.

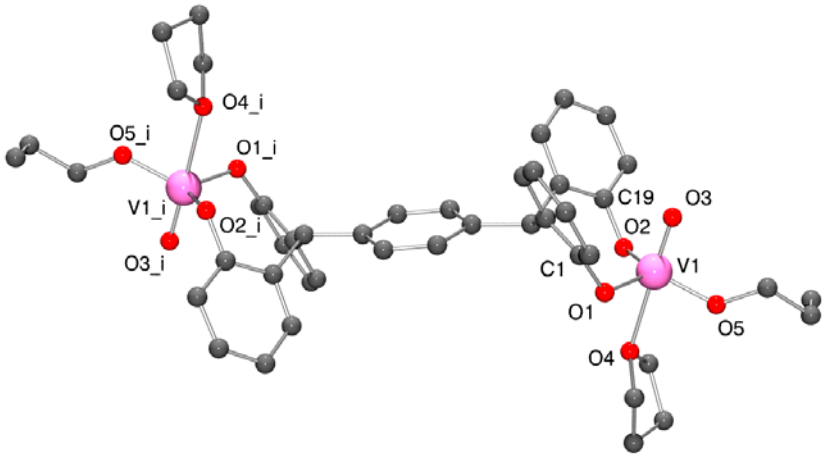

Figure 1. Representation of the centro-symmetric molecular structure of complex **1** in the solid state, indicating the atom numbering scheme. *tert*-Butyl groups, hydrogen atoms, and unbound solvent molecules have been removed for clarity. Selected bond lengths (Å) and angles (°): V1–

O3 1.5871(14), V1–O5 1.7878(15), V1–O2 1.8187(15), V1–O1 1.8256(16), V1–O4 2.3307(13), O3–V1–O5 100.20(7), O3–V1–O2 100.05(7), O5–V1–O2 119.29(7), O3–V1–O1 99.63(7), O5–V1–O1 120.16(7), O2–V1–O1 111.73(7), O3–V1–O4 178.12(7), O5–V1–O4 78.36(6), O2–V1–O4 81.73(6), O1–V1–O4 80.16(6). Symmetry operation used to generate equivalent atoms: i = 1−*x*, −*y*, −*z*.

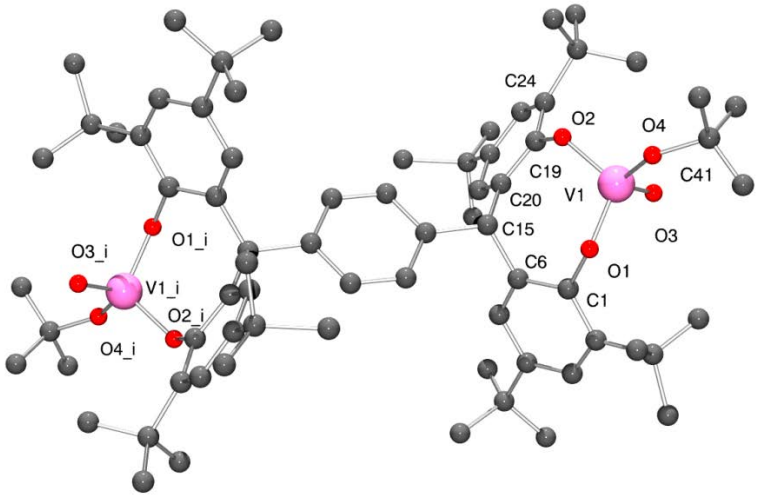

Figure 2. Representation of the centro-symmetric molecular structure of complex **2** in the solid state, indicating the atom numbering scheme. Hydrogen atoms, and unbound solvent molecules have been removed for clarity. Selected bond lengths (Å) and angles (°): O1–V1 1.725(6), O2–V1 1.786(5), O3–V1 1.547(6), O4–V1 1.682(7), O3–V1–O4 112.4(4), O3–V1–O1 106.8(3), O4–V1–O1 110.1(3), O3–V1–O2 106.1(3), O4–V1–O2 109.3(3), O1–V1–O2 112.0(2). Symmetry operation used to generate equivalent atoms: i = 1−*x*, 1−*y*, −*z*.

In complex **2**, each vanadyl centre is bound by the bi-dentate di-phenolate, forming an 8-membered metallocycle with a bite angle at the metal of 112.0(2) °. The coordination is completed by a single *tert*-butoxide ligand to form a slightly distorted tetrahedral geometry. The complex is centrosymmetric (Figure 2; for ORTEP diagram see Figure S2 in the ESI) with the

two vanadyl cations lying on opposite sides of the plane of the central phenyl ring in similar fashion to **1**.

Synthesis and structure of m-L^2H_4 derived vanadyl complexes: Similar treatment of the *meta* ligand L^2H_4 with a slight excess of [VO(O*n*Pr)$_3$] led to the formation of the complex {[VO(O*n*Pr)]$_2$(μ-*m*-L^2)} (R = *n*Pr (**3**)). The IR spectra contain a strong band at *ca* 990 cm^{-1} assigned to the *v*(V=O) mode. Unsurprisingly, the ^{51}V NMR spectrum is very similar to that of **1** with a single peak at δ -432.5 with $\omega_{½}$ 170 Hz (*cf* -433.3 ppm, $\omega_{½}$ 170 Hz for **1**); see Table S5 for all ^{51}V NMR spectroscopic data. Crystals of **3** suitable for an X-ray diffraction study were obtained on cooling of a THF/light petroleum solution to –20 ^{o}C. A tiny orange platelet was extracted from the solid product. This was examined at 100 K using synchrotron radiation (DLS beam-line I19, λ = 0.6889 Å). [14] The crystal was extremely weakly scattering and no significant diffraction was obvious beyond *ca*. 2θ = 36 °. It proved possible to solve the structure using direct methods and the chemical connectively is unequivocally established (Figure 3; for ORTEP diagram see Figure S3 in the ESI). No data beyond 36 ° were used in the structure refinement.

The structure contains two independent units that are chemically identical. Each is formed of one half of a molecule of $\mathbf{L^2}$. The second half is generated by symmetry. Each symmetry unique fragment is based upon bidentate coordination of $\mathbf{L^2}$ to the vanadyl cation $(V=O)^{2+}$. Coordination about the vanadyl is completed by tetrahydrofuran and *n*-propoxide to give trigonal bipyramidal geometry about the V center. There is some evidence for disordered solvent between these coordination complexes but we have not been able to resolve this.

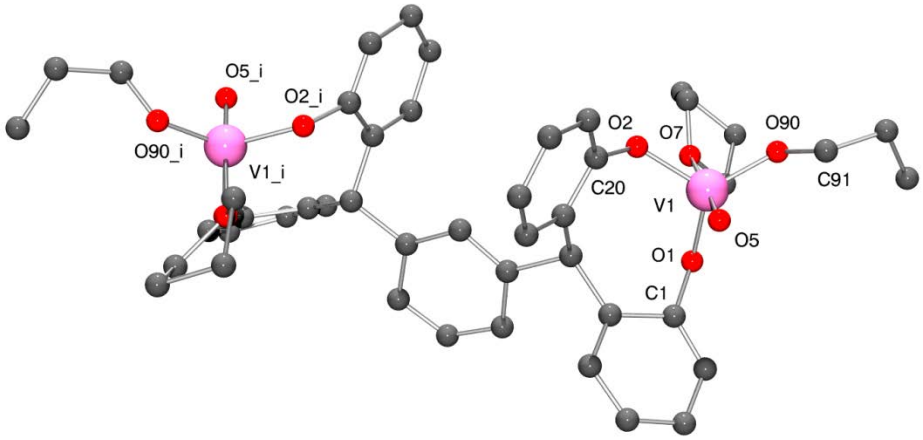

Figure 3: One of the symmetry unique complexes within **3** showing the *meta* arrangement in ligand $\mathbf{L^2}$. Tertiary butyl groups and hydrogen atoms have been omitted for clarity. Symmetry equivalent atoms are generated by the operator i = ½−x, y, ½−z.

Synthesis and structure of oxo-imido complexes: The effective use of (imido)vanadium complexes as pre-catalysts for α-olefin polymerization has been noted previously. [15] Given this, we have also explored possible routes to accessing imido-containing vanadium complexes of the tetra-phenol ligand set.

Treatment of the *para* ligand L^1H_4 with a slight excess of [V(N*p*-$R^1C_6H_4$(O*t*Bu)$_3$] (R^1 = Me, CF_3) led to the formation of the oxo-imido complexes {[VO(*t*BuO)][V(N*p*-$R^1C_6H_4$)(*t*BuO)](μ-*p*-L^1)} (R^1 = Me, **4**; CF_3, **5**). Crystals of **4** and **5** suitable for an X-ray diffraction study were obtained on prolonged cooling of a saturated dichloromethane solution (to –20 ^oC). The molecular structures are shown in Figures 4 and 5 (for ORTEP diagrams see Figures S4 and S5 in the ESI), with selected bond lengths (Å) and angles (^{o}) given in Table 2. For **4**, each vanadium center adopts a pseudo-tetrahedral geometry, with bond angles in the range 106.7(2) – 112.1(2) ^{o}. The molecule is centro-symmetric. Each 8-membered metallocycle adopts the boat conformation, and the bite angle of the chelate at each end is 111.80(18) ^{o}. The *tert*-butoxide ligand is again somewhat bent

[V1 – O4 – C40 = 144.5(4) ^{o}], whilst the organoimido group is near linear [V1 – N1 – C45 = 172.8(6) ^{o}].

In the case of **5**, the molecule also lies on a center of symmetry and so again half is unique. There is therefore disorder such that at V1 there is a 50/50 mixture of (i) a vanadyl and an unbound CH_2Cl_2 molecule and (ii) the *p*-arylimido group. We interpret this as being (i) at one end and (ii) at the other but that the arrangement is not regular throughout the crystal. As in **4**, the organoimido group is near linear [V1 – N1 – C1 = 173.4(6) ^{o}], whereas the alkoxide is bent [V1 – O1 – C8 144.3(5) ^{o}]. The vanadyl group is involved in H-bonding to a solvent molecule (CH_2Cl_2) with the geometrical parameters H45A ··· O4 = 2.20 Å, angle at H45 = 167 ^{o}, H45B ··· centroid of C30 - C35 = 2.85 Å, angle at H45B = 136 ^{o}. Molecules of **6** pack into chains but there are no significant interactions between molecules and chains.

Table 2. Selected bond lengths for **4**·$2CH_2Cl_2$ and **5**·$2CH_2Cl_2$

Bond lengths (Å)/Angles (^{o})	**4**·$2CH_2Cl_2$	**5**·$2CH_2Cl_2$
V1−N1	1.600(5)	1.603(5)
V1−O1	1.735(4)	1.734(5)
V1−O2	1.805(4)	1.803(5)
V1−O3	1.797(4)	1.802(4)
V1–O1–C8	144.4(4)	144.3(5)
V1–O2–C12	125.7(4)	126.0(4)
V1–O3–C30	127.5(4)	125.2(4)
O1–V1–N1	112.1(2)	111.8(3)

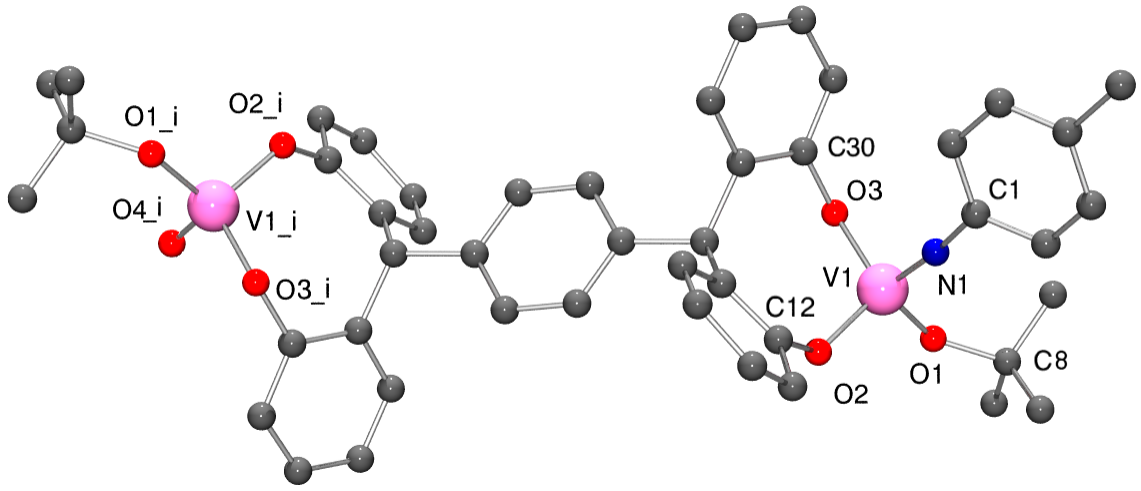

Figure 4. Molecular structure of complex **4**·2CH_2Cl_2, indicating the atom numbering scheme. *tert*-Butyl groups, hydrogen atoms, and unbound solvent molecules have been removed for clarity. Symmetry equivalent atoms are generated by the operator i = 1−x, 1−y, 2−z.

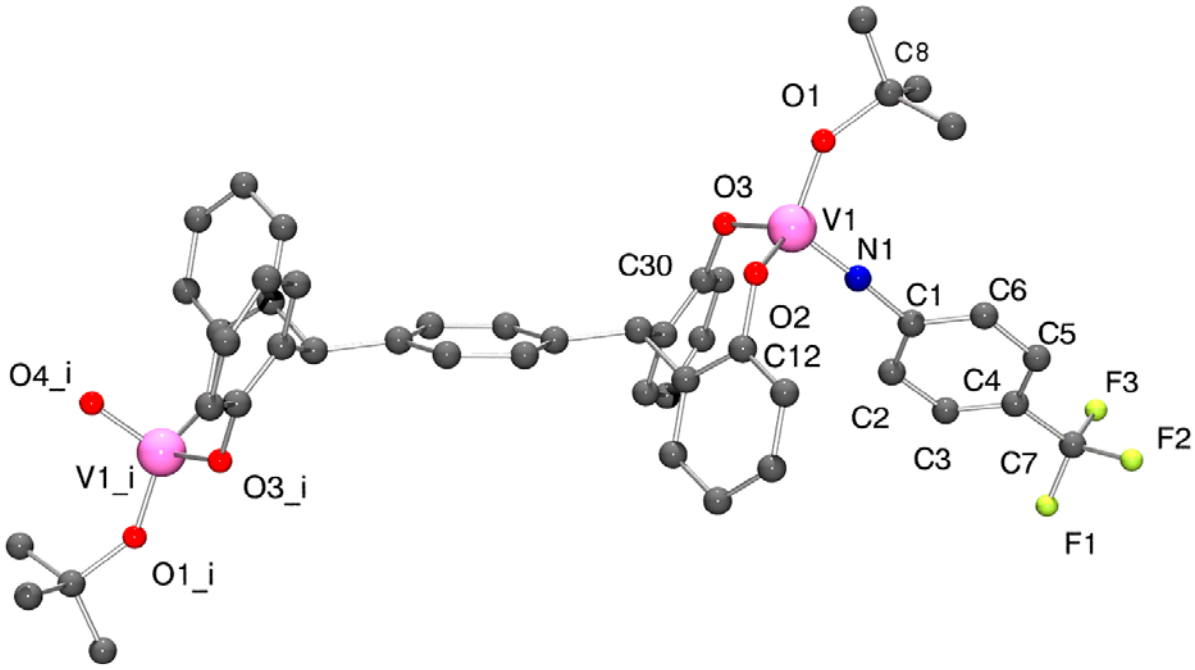

Figure 5. Molecular structure of complex **5**·2CH_2Cl_2, indicating the atom numbering scheme. *tert*-Butyl groups, hydrogen atoms, and unbound solvent molecules have been removed for

clarity. Symmetry operation used to generate equivalent atoms: i = 1−*x*, 1−*y*, 1−*z*.

Synthesis and structure of bis-imido complexes: Given the sensitive nature of the *tert*-butoxides employed above, we turned out attention to use of the parent trichlorides, namely [V(N*p*-$R^1C_6H_4$)Cl_3]. [16]

Interaction of [V(N*p*-MeC_6H_4)Cl_3] with the sodium salt *p*-L^1Na_4 afforded the complex {[V(N*p*-MeC_6H_4)(THF)Cl]$_2$(μ-*p*-L^1)} (**6**·4toluene) as a red/brown crystalline solid. The molecular structure of **6**·4toluene is shown in Figure 6 (for ORTEP diagram see Figure S6 in the ESI), with selected bond lengths and angles given in the caption. The geometry at vanadium is best described as trigonal bipyramidal with the imido and THF groups occupying axial positions [N(1) – V(1) – O(3) 175.11(16) ^{o}]. Distortions are in the range 110.17(12) – 123.9(2) ^{o}, with the largest deviation associated with the angle subtended at the metal by the phenolic oxygen centers; the metallocycle adopts a boat conformation. The imido ligand has the geometrical parameters associated with a linear imido function [V(1) – N(1) 1.656(4) Å; V(1) – N(1) – C(50) 170.4(3) ^{o}].

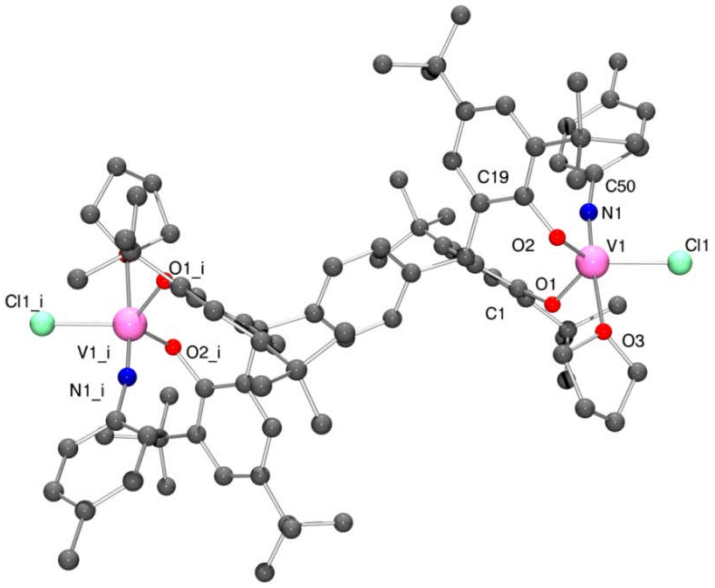

Figure 6. Molecular structure of complex **6**·4toluene, indicating the atom numbering scheme. Hydrogen atoms have been removed for clarity. Selected bond lengths (Å) and angles (°): V(1)–N(1) 1.656(4), V1–O1 1.819(3), V1–O2 1.817(3), V1–O3 2.189(3), V1–Cl1 2.2814(14); O1–V1–N1 98.84(15), O1–V1–O2 110.17(12), Cl1–V1–N1 92.89(12), V1–O1–C1 126.9(2), V1–O2–C19 120.6(3), V1–N1–C50 170.4(3). Symmetry operation used to generate equivalent atoms: i = −*x*, 1−*y*, −z.

Similar use of $[V(N\textit{p}\text{-}CF_3C_6H_4)Cl_3]$ with L^1H_4 led to the isolation of $\{[V(N\textit{p}\text{-}CF_3C_6H_4)(THF)Cl]_2(\mu\text{-}\textit{p}\text{-}L^1)\}$ (**7**) in moderate yield (*ca.* 47 %). Crystals suitable for X-ray diffraction were obtained from a saturated solution of acetonitrile at ambient temperature. Although the data are not of the best quality, the connectivity is clear and the molecular structure is shown in Figure 7 (for ORTEP diagram see Figure S7 in the ESI). In the ^{51}V NMR spectra of **4** and **5** there are two peaks (see table S5); imido peaks are usually found downfield of their

vanadyl counterparts. [16]

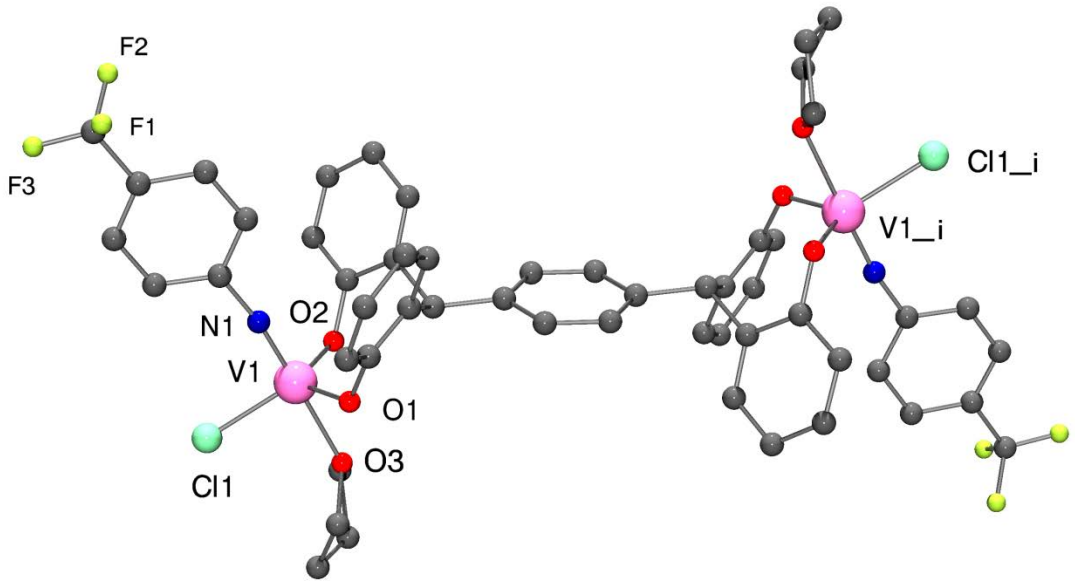

Figure 7. Molecular structure of complex **7**, indicating the atom numbering scheme. Hydrogen atoms and *tert*-butyl groups have been removed for clarity. Selected bond lengths (Å) and angles (°): V(1)–N(1) 1.666(4), V1–O1 1.808(3), V1–O2 1.819(3), V1–O3 2.210(3), V1–Cl1 2.2625(14); O1–V1–N1 99.05(18), O1–V1–O2 112.47(14), Cl1–V1–N1 95.29(14), V1–O1–C1 122.7(3), V1–O2–C19 121.5(3), V1–N1–C34 172.0(4).

Under the conditions employed herein, on several occasions, small amounts of spiro-type compounds containing the motif **I** (see Figure 8) were isolated. In particular, the spiro compound with X = *t*Bu was isolated from the reaction employing [V($NC_6H_4CF_3$-*p*)Cl_3], whilst that with X = Cl resulted from attempts to form a vanadyl chloride complex of *p*-L^1H_4 using [$VOCl_3$]. The crystal structures of both spiro compounds are presented in the ESI (see Figures S8 and S9 and Tables S1-4). A search of the Cambridge Crystallographic Database (CSD) for motifs related to **I** revealed 7 hits in calixarene type systems. [17, 18]

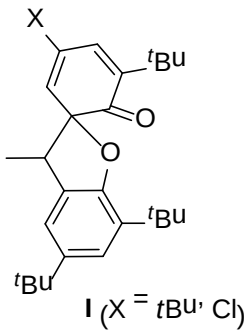

Figure 8. Spiro motif **I**.

Use of $\mathbf{L^3H_2}$: For comparative studies, we have also treated the potentially bidentate ligand $\mathbf{L^3H_2}$ with [VO(O*n*Pr)$_3$], which led to the formation of compound **8**. In the IR spectrum, a strong band at 989 cm^{-1} is assigned to the vanadyl group. Compound **8** was crystallized from light petroleum to give red needles which were suitable for single crystal X-ray diffraction. The crystal structure revealed that compound **8** forms a dimeric structure in the solid state (see Figure 9; for ORTEP diagram see Figure S10 in the ESI). The vanadium oxytri-*n*-propoxide loses two equivalents of propanol on binding to the bidentate ligand. The dimer is centrosymmetric and contains two vanadyl moieties in a *trans* arrangement that are bridged by the two remaining *n*-propoxide ligands. Each vanadium metal center is in trigonal bipyramidal geometry; the bidentate ligand and one of the *n*-propoxide ligands occupying the equatorial position, the vanadyl oxygen and second *n*-propoxide occupies the axial position. The di-phenolate ligand's third phenol ring is rotated away with the methine hydrogen directed toward the vanadium center. Unlike for complexes **1** and **3** which contain terminal *n*-propoxide ligands, the presence of the bridging *n*-propoxides in **8** together with the bulky chelate ligand appears to prevent ligation by THF. As in the tetra-phenolate systems above, the 8-membered metallocycle in **8** adopts a boat conformation, for which the bite angle subtended at vanadium is 113.14(7) ^{o}. A search of the CSD for use of di-

phenols with an aryl group bound at the bridging carbon afforded 114 hits for metal complexes, however most of these were either based on tripodal ligands or where the motif of interest formed part of a more exotic ligating species. Indeed, there was only one example of the previous use of the parent $\mathbf{L^3H_2}$, which was a report of its utilization in titanium chemistry. [17, 19]

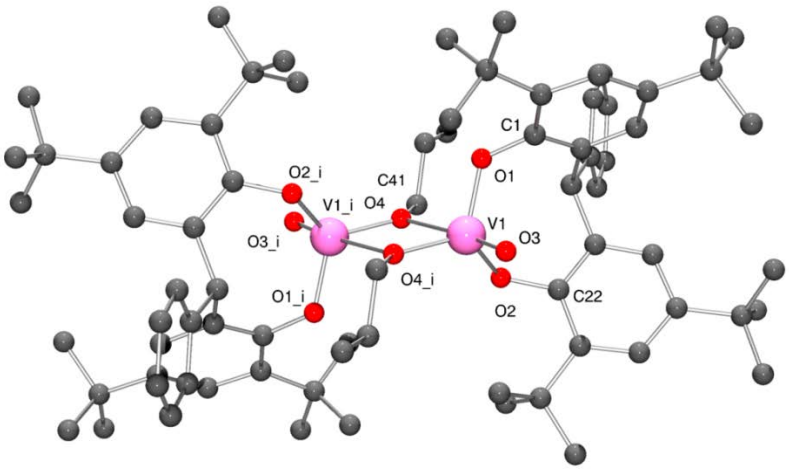

Figure 9. Representation of the molecular structure of complex **8**, indicating the atom numbering scheme. For clarity, hydrogen atoms have been removed. One of the symmetry independent *t*-butyl groups is disordered over two positions. Selected bond lengths (Å) and angles (°): O1–V1 1.8117(15), O2–V1 1.8165(16), O3–V1 1.5869(15), O4–V1^i 1.8348(15), O4 –V1 2.2917(14), V1–O4^i 1.8348(15), V1^i–O4–V1 108.23(6), O3–V1–O1 100.19(7), O3–V1–O2 100.58(8), O1–V1–O2 113.14(7), O3–V1–O4^i 100.35(7), O1–V1–O4^i 115.74(7), O2–V1–O4^i 121.56(7), O3–V1–O4 172.06(7), O1–V1–O4 84.55(6), O2–V1–O4 83.19(6), O4^i–V1–O4 71.77(6). Symmetry equivalent atoms are generated by the operator i = 1−x, 1−y, 2−z.

Ethylene Polymerization Screening

Compounds **1** - **3**, **5** - **8** and [VO(OEt)Cl_2], were screened for the polymerization of ethylene. Each catalyst has been screened for polymerization using different co-catalysts (DMAC, Dimethylaluminium chloride; DEAC, diethylaluminium chloride; EADC, ethylaluminium dichloride; EASC, ethylaluminium sesquichloride) and with addition of ETA (ethyltrichloroacetate). From the co-catalyst screening (Tables 3, S6, S7 and Figures S11-S46 in the ESI; for use of Me_3Al, Et_3Al and DMAO (dried MAO – see general experimental), see Tables S8 and S9, ESI), the addition of ETA to the catalytic system is beneficial; the activity of the runs including an addition of ETA was always higher than with no addition (Table 3). [20] In all cases, the addition of larger equivalence of ETA and co-catalyst lead to improved activity. Use of different chloro-aluminium alkyls indicated, for compound **1**, that DEAC was the co-catalyst of choice giving the highest activity and lowest molecular weight distribution (Table 3, run 4); compound **3** gave similar activities for each co-catalyst (*ie* no advantage of meta *versus* para ligation), whereas surprisingly, given the similarities with **3**, compound **8** gave much higher activities when using the ethyl derived aluminium chloride co-catalysts (see Table 3, runs 20 – 27). For compounds **1** and **3**, EADC and EASC gave lower activities than DEAC and lower molecular weights than DMAC. The highest molecular weight polyethylene was obtained using DMAC as co-catalyst; however the PDI values were high for each pre-catalyst employed suggesting multiple active species.

Table 3. Selected results for the effect of co-catalyst and ETA on compounds **1** - **3**, **5**, **8** and **[VO(OEt)Cl_2]**.[a]

Run	Pre-Cat	Co-Cat	Al/V	ETA/V	T[c]	Yield[b]	Activity[d]	M_w	M_n	PDI
1	**1**	DMAC	20000		30	0.128	12,800	2,261,718	547,734	4.1
2			20000	20000	30	0.534	53,400	974,413	116,671	8.4

3		DEAC	20000		30	0.009	900	455,970	88,930	5.1
4			20000	20000	10[e]	0.811	243,400	73,074	25,671	2.9
5		EADC	20000		30	0.05	5,000	228,678	94,326	2.4
6			20000	20000	30	0.338	33,800	749,498	205,539	3.7
7		EASC	20000		30	0.058	5,800	943,144	353,483	2.7
8			20000	20000	30	0.358	35,800	666,983	160,727	4.2
9	**2**	DMAC	20000	20000	30	0.306	122,200	1,180,000	241,000	4.9
10		DEAC	20000	20000	30	0.231	92,300	1,040,000	103,000	10.0
11	**3**	DMAC	20000		30	0.112	11,200	3,290,580	1,349,253	2.44
12			20000	20000	30	0.45	45,000	865,647	81,817	10.6
13		DEAC	20000	20000	30	0.494	49,400	267,660	45,443	5.9
14		EADC	20000		30	0.01	1000	196,554	57,342	3.4
15			20000	20000	30	0.472	47,200	749,897	70,411	10.6
16		EASC	20000		30	0.034	3,400	967,997	315,747	3.1
17			20000	20000	30	0.438	43,800	273,709	27,818	9.8
18	**5**	DMAC	20000	20000	30	0.256	102,200	814,000	123,000	6.6
19		DEAC	20000	20000	30	0.237	94,700	933,000	88,800	10.5
20	**8**	DMAC	20000		30	0.341	34,100	1,683,732	57,625	29.2
21			20000	20000	30	0.423	42,300	1,067,563	120,753	8.84
22		DEAC	20000		30	0.039	3,900	333,763	104,963	3.2
23			20000	20000	15[e]	0.527	105,400	110,765	26,097	4.2
24		EADC	20000		30	0.0107	1,100	181,151	68,551	2.6
25			20000	20000	23[e]	0.538	70,200	547,756	135,546	4.0
26		EASC	20000		30	0.0305	3,100	874,365	191,854	4.6
27			20000	20000	22[e]	0.4951	67,500	216,581	29,627	7.3
28	**[VO(OEt)Cl_2]**	DMAC	20000		30	0.106	21,200	2,114,696	740,175	2.9
29			20000	20000	30	0.429	85,800	1,787,338	385,401	4.6
30		DEAC	20000	20000	30	0.343	68,600	139,330	48,676	2.9
31		EADC	20000	20000	30	0.375	37,500	711,232	187,694	3.8

32	EASC	20000	20000	30	0.341	34,100	387,638	99,975	3.9

[a] **Conditions**: 50 °C, 5 mL toluene, 0.01 µmol V, 0.8 MPa ethylene, reaction quenched with isobutyl alcohol; [b] grams, [c] minutes, [d](g/(mmol.h)), [e] polymerization was stopped due to consumption of stock ethylene. See ESI for full screening results – Table S5.

Comparison of the observed catalytic activities and molecular weights (M_w) for the dinuclear vanadyl complexes bridged with a tetra-phenolate ligand *versus* the *n*-propoxide bridged vanadyl complex **8** revealed that the use of different co-catalysts as well as the presence or absence of ETA played a significant role. For example, in the presence of ETA, all tetra-phenolate bridged systems were more active than the *n*-propoxide bridged vanadyl complex **8**, however the polyethylene produced via **8**/ETA tended to be of higher molecular weight (M_w). In the absence of ETA, **8**/DMAC exhibited higher activities than did the tetra-phenolate bridged systems, although in this case, the polyethylene was of higher molecular weight for the tetra-phenolate bridged systems. The use of DEAC as co-catalyst generally afforded the same trends as DMAC for **1**, whereas for **2**, **3** and **5** with ETA, the activities were less than observed for **8**/ETA; molecular weights were higher for the tetra-phenolate bridged systems. With EADC or EASC, activities in the presence of ETA were higher for **8**, but molecular weights for the PE obtained were higher for the tetra-phenolate bridged systems. In the absence of ETA, activities for **1** were higher than for **8**, whilst for **3** they were about the same as those observed for **8**; molecular weights for the PE obtained were higher for the tetra-phenolate bridged systems.

Using the conditions established in Table 3 (20,000 equivalence DEAC or DMAC, 20,000 equivalence ETA) compounds **1** - **3**, **5** - **8** and the reference compound [$VO(OEt)Cl_2$] were screened over a series of temperatures (Tables 4 and S7 and Figures S27-S42 in the ESI). When

DMAC was used as co-catalyst, the vanadyl-containing pre-catalysts **1 - 3**, **5** and [VO(OEt)Cl_2] showed optimal activity at 50 °C, whereas the *n*-propoxide bridged pre-catalyst **8** is thermally more stable and gave highest activity at 80 °C; each compound except for compound **8** showed lower PDI values at 80 °C. In the runs where DEAC was employed as co-catalyst again 50 °C was the temperature of choice, except for compound **1** where a temperature of 80 °C showed increased activity.

For the non-vanadyl (imido) pre-catalysts **6** and **7**, observed activities were higher when employing DEAC *versus* DMAC at 50 ^{o}C, with activities as high as 236,000 g/(mmol.hr) (29.5 Kg PE/mmolV.h.bar) recorded; pre-catalyst **6** bearing the *p*-tolyl groups gave higher activities than **7** bearing the *p*-CF_3 group at 50 ^{o}C for both DMAC and DEAC. At 80 ^{o}C, the activities fell off dramatically when using either DMAC or DEAC, with no products isolated at the higher temperatures of 100 and 144 ^{o}C. Indeed, the fall-off in the observed activity was far steeper for these imido systems than was observed for any of the vanadyl systems. The molecular weights of the polymers isolated at 50 and 80 ^{o}C were higher when obtained in the presence of DMAC, and in the case of **6** at 50 ^{o}C, were larger than any of the molecular weights (M_w) observed herein when using the vanadyl complexes. However, the molecular weights (M_w) of the PE obtained using **6** or **7** in combination with DEAC/ETA were much lower than those observed when employing the vanadyl complexes under similar conditions.

Table 4. Effect of temperature on compounds **1 - 3**, **5 - 8** and [VO(OEt)Cl_2].[a]

Run	Pre-Cat	Co-Cat	Temp[c]	T[d]	Yield[b]	Activity[e]	M_w	M_n	PDI	T_m[c]
1	**1**	DMAC	50	30	0.422	168,800	467,300	67,300	6.9	137.2
2			80	30	0.41	163,900	136,100	44,500	3.1	133.2
3		DEAC	50	30	0.283	113,200	254,000	38,900	6.5	135.4
4			80	30	0.355	14,8000	135,800	20,600	6.7	136.1

5	**2**	DMAC	50	30	0.306	122,200	1,180,000	241,000	4.9	136.1
6			80	30	0.217	86,800	249,000	26,800	9.3	136.0
7		DEAC	50	30	0.231	92,300	1,040,000	103,000	10.0	131.8
8			80	30	0.110	44,100	82,000	18,800	4.4	134.3
9	**3**	DMAC	50	30	0.357	142,800	536,200	93,900	5.7	132.0
10			80	30	0.301	120,600	173,800	60,400	2.9	133.0
11		DEAC	50	30	0.218	87,400	555,100	84,000	6.6	134.0
12			80	30	0.046	18,400	366,500	34,900	10.5	133.0
13	**5**	DMAC	50	30	0.256	102,200	814,000	123,000	6.6	131.9
14			80	30	0.224	89,700	163,000	44,800	3.6	133.5
15		DEAC	50	30	0.237	94,700	933,000	88,800	10.5	132.2
16			80	30	0.040	16,200	142,000	16,100	8.8	133.1
17	**6**	DMAC	50	30	0.3099	124,000	1,430,000	265,000	5.4	136.8
18			80	30	0.034	13,600	119,000	30,800	3.8	134.3
19		DEAC	50	30	0.5899	236,000	162,000	62,800	2.6	135.1
20			80	30	0.1439	57,600	65,800	35,000	1.9	134.1
21	**7**	DMAC	50	30	119.84	119,800	996,000	132,000	7.5	134.3
22			80	30	32.56	32,600	131,000	52,800	2.5	133.7
23		DEAC	50	30	0.4856	194,200	173,000	58,600	3.0	134.6
24			80	30	0.0709	28,400	72,400	39,500	1.8	133.6
25	**8**	DMAC	50	30	0.311	124,400	783,800	115,000	6.8	
26			80	30	0.402	161,000	188,000	67,800	2.8	
27		DEAC	50	30	0.215	86,100	671,700	88,100	7.6	
28			80	30	0.056	22,600	313,500	35,800	8.8	

29	**[VO(OEt)Cl_2]**	DMAC	50	30	0.374	74,700	945,800	168,700	5.6	134.7
30			80	30	0.354	70,800	137,600	45,700	3.0	133.3
31		DEAC	50	30	0.483	96,700	316,500	56,800	5.6	134.4
32			80	30	0.237	47,400	208,700	27,200	7.7	134.0

[a] **Conditions**: 5 mL toluene, 0.005 µmol V, 0.8 MPa ethylene, 20,000 equivalents Co-catalyst, 20,000 equivalents ETA, reaction quenched with *iso*-butyl alcohol; [b] grams, [c] °C, [d] minutes, [e] (g/(mmol.h)).

The polyethylene formed is highly linear, with melting points in the range 130.2 - 137.2 °C, and no branching could be assigned from the ^{13}C NMR spectra (for example, see Figure S43 in the ESI for catalyst system using **2**/Et_3AlCl_2 – run 31, Table S6). [21]

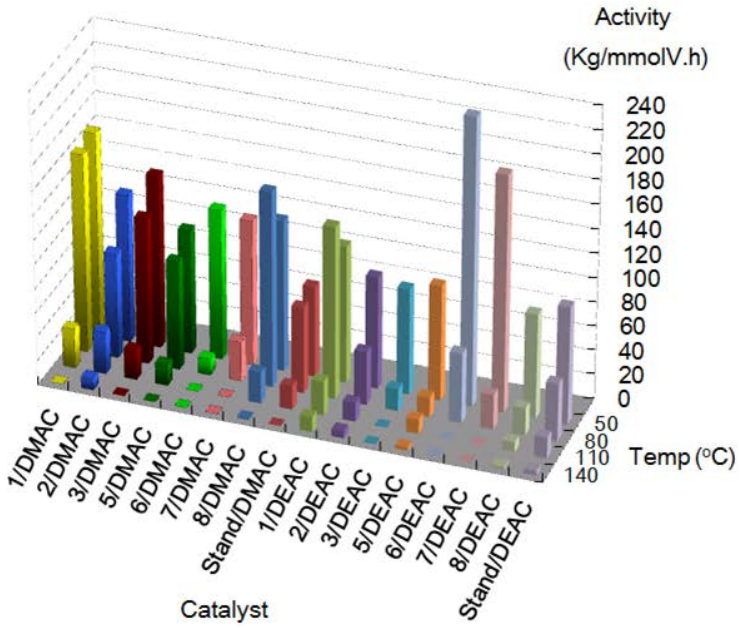

Figure 10. Activity (x 10^3 g(mmol(V)h)$^{-1}$) in ethylene polymerization at 50 – 140 °C by [VO(OEt)Cl_2], **1** – **3**, **5** - **8**.

Screening using Me_3Al, Et_3Al or DMAO as co-catalysts in the presence of ETA proved unsuccessful (see tables S8 and S9, ESI), *i.e.* such systems were inactive under the conditions employed herein. We note that improved activities in vanadium-based systems in the presence of chloroaluminium co-catalysts have previously been associated with the presence of V-Cl-Al type motifs present in the active species, [2b] and with the nature of the ion-pair formed. Smaller co-catalysts such as DMAC or DEAC *versus* MAO are capable of equilibria involving chloro-bridged species and discrete ions. [22]

Ethylene/Propylene Co- Polymerization Screening

The co-polymerization of propylene and ethylene using compounds **1 - 3**, **5 - 8** and $[VO(OEt)Cl_2]$ at 50 °C revealed (see Table 5 and Figures S44-S46 in the ESI) that DMAC, in combination with the vanadyl-containing pre-catalysts, was a more efficient co-catalyst than DEAC, achieving an activity greater than 100,000 g/mmol.h for pre-catalysts **1**, **3**, **8** and $[VO(OEt)Cl_2]$. As for the homo-polymerization of ethylene, there was no advantage observed for the co-polymerization results herein when using a *meta* ligand framework over *para* ligation (**1** v **3**), despite the increased possibility of the former to bring the metals into closer proximity.

For the non-vanadyl systems **6** and **7**, the activity observed was higher when using DEAC as co-catalyst, with the system employing pre-catalyst **6** achieving an activity of the order of 111,400 g/mmol.h. In all cases, the molecular weight (M_w) of the co-polymer produced was much higher when DMAC was employed as co-catalyst. In each run, the PDI values were typically in the range 1.8 – 2.8 (the exception was run 8). When using DMAC, the propylene incorporation for the vanadyl-containing systems was between 7.5 – 8.6 % (7.2 – 8.5 % for DEAC), whereas for

the imido-containing systems, the incorporation was somewhat lower at 3.8 – 4.7 % (DMAC) and 4.0 – 7.4 % (DEAC). For the *n*-propoxide complex **8**, propylene incorporation was similar to the other vanadyl complexes [8.2 % DMAC and 7.7 % DEAC], whilst the C3 incorporation for the standard catalyst [$VO(OEt)Cl_2$] was slightly higher at 10.0 % (DMAC) and 9.1 % (DEAC).

Table 5. Ethylene/propylene co-polymerizations using compounds **1 - 3**, **5 - 8** and [$VO(OEt)Cl_2$].[a]

Run	Pre-Cat	Co-Cat	Yield[b]	Activity[c]	%C3[d]	M_w	M_n	PDI	T_m[e]
1	**1**	DMAC	0.361	144,400	8.5	325,200	133,600	2.4	90.4
2		DEAC	0.203	81,000	8.3	88,800	46,400	1.9	93.4
3	**2**	DMAC	0.145	57,880	8.6	217,100	100,500	2.2	86.6
4		DEAC	0.084	33,480	7.2	78,000	40,300	1.9	91.6
5	**3**	DMAC	0.338	135,100	8.2	291,100	123,100	2.4	90.9
6		DEAC	0.116	46,400	7.6	98,300	43,200	2.3	95.0
7	**5**	DMAC	0.214	85,560	7.5	241,200	103,800	2.3	89.1
8		DEAC	0.171	68,240	8.5	87,200	42,800	8.5	89.9
9	**6**	DMAC	0.082	32,960	4.7	301,900	123,900	2.4	89.6
10		DEAC	0.278	111,360	7.4	108,000	53,700	2.0	88.2
11	**7**	DMAC	0.099	39,440	3.8	289,500	117,800	2.5	86.8
12		DEAC	0.199	79,760	4.0	102,400	53,800	1.9	84.5
13	**8**	DMAC	0.274	109,600	8.2	311,300	136,900	2.3	90.9
14		DEAC	0.189	75,600	7.7	99,300	53,000	1.9	93.6
15	**[$VO(OEt)Cl_2$]**	DMAC	0.391	156,200	10.0	241,100	86,600	2.8	88.9
16		DEAC	0.191	76,400	9.1	75,700	42,700	1.8	90.2

[a] **Conditions**: 5 mL toluene, 30 minutes, 50 °C, 0.005 µmol V, 0.4 MPa ethylene, 0.4 MPa propylene, 20,000 equivalents co-catalyst, 20,000 equivalents ETA, reaction quenched with isobutyl alcohol; [b]grams, [c](g/(mmol.h)), [d] Mol% determined by IR. [e] °C.

Whilst the catalytic activities of the systems described herein (see Figure 15) are amongst the highest yet reported for ethylene/propylene co-polymerization for vanadium-based systems, the degree of propylene incorporation [3.8 – 8.6 mol%] is far lower than other reported systems; typically other systems incorporate between 15 – 40 mol% C3. [4b-d, 11]

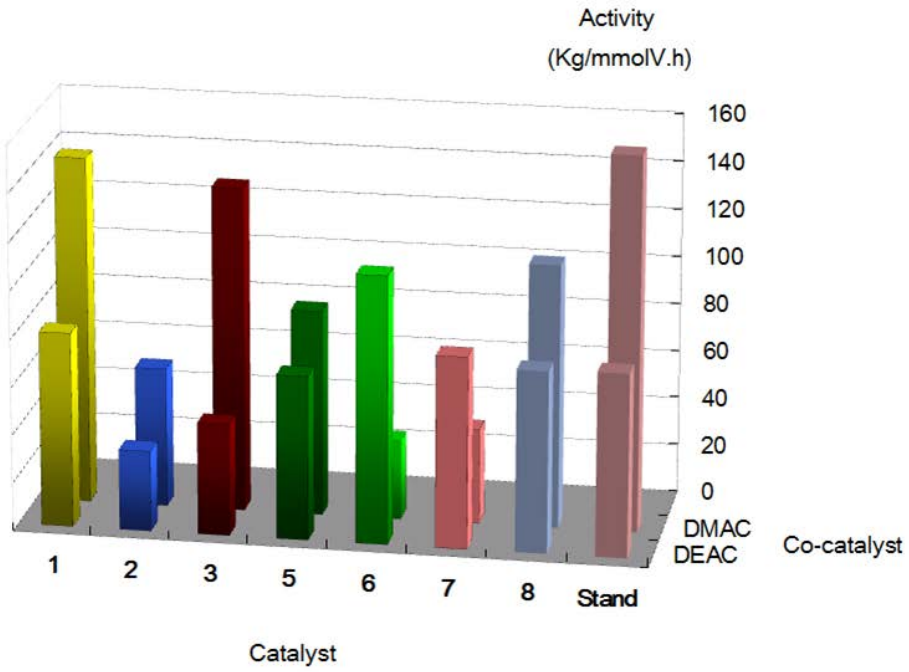

Figure 11. Activity (x 10^3 g(mmol(V)h)$^{-1}$) in ethylene/propylene co-polymerization at 50 ^{o}C by [VO(OEt)Cl_2], **1** – **3** and **5** – **8** in the presence of DMAC or DEAC as co-catalyst.

In conclusion, the *para* or *meta*-tetra-phenols *p*-L^1H_4 or *m*-L^2H_4 on reaction with [V(X)$(OR)_3$] (X = oxo or imido) allow access to two new families of bimetallic complexes capable of ethylene polymerization with high activity bearing either two vanadyl centers or a combination of a vanadyl/vanadium imido center. Access to bimetallic complexes possessing two vanadium imido

centers was achieved using the imido trichloride precursors of the type [V(NAr)Cl_3] (Ar = *p*-tolyl, *p*-$CF_3C_6H_4$) via either salt metathesis or HCl elimination.

The tetra-phenolate vanadyl complexes **1** – **3** and **5**, when activated with DMAC or DEAC/ETA, showed higher activities than the benchmark catalyst [VO(OEt)Cl_2] for ethylene polymerization; better performances were observed in the presence of DMAC. No advantages were observed when employing *meta versus* the *para* ligation. The non-vanadyl (imido) complexes **6** and **7** performed better in the presence of DEAC and at 50 ^oC achieved activities as high as 230,000 g/(mmol.hr), which is the highest activity reported to-date under such robust conditions. In the case of ethylene/propylene co-polymerization, the complexes described herein gave higher molecular weight copolymer than did [VO(OEt)Cl_2] at comparable activity. Large variation of catalytic activity and polymer (or co-polymer) molecular weight (M_w) was observed on variation of the co-catalyst employed and whether the re-activator ETA was present or not for the various types of vanadium pre-catalyst deployed herein. The extremely high activities observed for these vanadium-based systems suggest that they are of potential industrial use.

Experimental

General: All manipulations were carried out under an atmosphere of dry nitrogen using conventional Schlenk and cannula techniques or in a conventional nitrogen-filled glove box. Diethyl ether and tetrahydrofuran were refluxed over sodium and benzophenone. Toluene was refluxed over sodium. Dichloromethane and acetonitrile were refluxed over calcium hydride. All solvents were distilled and degassed prior to use. IR spectra (nujol mulls, KBr or NaCl windows) were recorded on a Nicolet Avatar 360 FT IR spectrometer; ^1H NMR spectra were recorded at

room temperature on a Varian VXR 400 S spectrometer at 400 MHz or a Gemini 300 NMR spectrometer or a Bruker Advance DPX-300 spectrometer at 300 MHz. The ^{1}H NMR spectra were calibrated against the residual protio impurity of the deuterated solvent. Elemental analyses were performed by the elemental analysis service at the London Metropolitan University. The ligand L^1H_4, L^2H_4 and L^3H_2 were prepared as described in the literature. [5, 23] The precursors $[V(N\textit{p}\text{-}RC_6H_4)(O\textit{t}Bu)_3]$ (R = Me, CF_3) were prepared via K*t*OBu using the method of Maatta. [16] For the polymerization studies, the dry toluene employed as a polymerization solvent was purified by passage through columns of activated alumina and BASF R3-11 oxygen scavenger. Methylaluminoxane (MAO) was purchased from Albemarle Corporation as a 1.2 M toluene solution. This solution was dried under vacuum to remove the toluene and a substantial fraction of the $AlMe_3$, to produce "dried MAO" (DMAO). Ethylene was obtained from Sumitomo Seika Co.

Synthesis of $\{[VO(O\textit{n}Pr)(THF)]_2(\mu\text{-}\textit{p}\text{-}L^1)\}\cdot 2(THF)$ (**1**·2(THF))

α,α,α′,α′-Tetrakis(3,5-di-*tert*-butyl-2-hydroxyphenyl)-*p*-xylene $\mathbf{L^1}H_4$ (4.1 g, 4.4 mmol) was dissolved in tetrahydrofuran (40 mL). Vanadium oxytri-*n*-propoxide (1.0 mL, 4.5 mmol) was added via syringe and the solution was stirred at room temperature for 16 h. The volatiles were removed *in vacuo,* and crystallization using THF/light petroleum gave orange plates of the compound **1** (2.6 g, 45 %). MS (EI, *m/z*) 1170.6 $[M\text{-}2THF]^+$, 1110.5 $[M\text{-}O\textit{n}Pr\text{-}2THF]^+$, 1068.5 $[M\text{-}\textit{n}Pr\text{-}O\textit{n}Pr\text{-}2THF]^{2+}$. IR (Nujol, KBr, cm^{-1}): 1597w, 1507m, 1435s, 1402w, 1286w, 1261m, 1221s, 1203s, 1153m, 1118s, 1104s, 1027s, 989s, 908m, 891m, 876s, 837s, 801m, 777m, 767m, 750m, 736w, 702w, 659s, 603m, 578w. Found: C, 71.61; H, 8.42. $C_{70}H_{100}O_8V_2$ (sample dried *in*

vacuo for 24 h leads to loss of THF x2) requires C, 71.77; H, 8.60 %. ^{1}H NMR ($CDCl_3$): δ = 7.31 (d, 4H, *J* = 2.33, aryl*H*), 7.22 (d, 4H, *J* = 2.33, aryl*H*), 6.78 (s, 4H, aryl*H*), 6.31 (s, 2H, Ar_3-C*H*), 5.36 (t, 4H, *J* = 6.00, OCH_2CH_2), 3.75 (bm, 8H, THF α-*H*), 1.98 (sextet, 4H, *J* = 6.73, $CH_2CH_2CH_3$), 1.86 (bm, 8H, THF β-*H*), 1.40 (s, 36H, *t*Bu), 1.24 (s, 36H, *t*Bu), 1.08 (t, 6H, *J* = 7.35, CH_2CH_3). ^{51}V NMR ($CDCl_3$): δ = -433.3 ($w_{1/2}$ =170 Hz).

Synthesis of {$\mathbf{L^1}$[VO(*t*BuO)]$_2$}·2MeCN (**2**·2MeCN)

$\mathbf{L^1}H_4$ (4.1 g, 4.4 mmol) and [VO(*t*BuO)$_3$] (3.20 g, 8.90 mmol) were refluxed in toluene (30 ml) for 12 h. On cooling, volatiles were removed *in-vacuo* and the residue can be extracted into either acetonitrile or dichloromethane (30 ml). Prolonged standing at 0 ^{o}C afforded **2** as a brown solid in 66 % (3.72 g) yield. $C_{72}H_{104}V_2O_8·0.75CH_2Cl_2$ (sample dried *in-vacuo* for 2 h) requires C 69.17, H, 8.42. Found C, 68.84, H 8.77 %. MS (solid, APCI) [24]: *m/z* 1199.6 $[M]^+$, 1125.6 [M-O*t*Bu]$^+$, 1069.5 [M-O*t*Bu-*t*Bu]$^{2+}$. IR: 1594w, 1568w, 1508w, 1401m, 1291m, 1261s, 1236m, 1224s, 1211m, 1200m, 1153s, 1118s, 1104s, 1021m, 1004s, 969bs, 911m, 876s, 845s, 826w, 800m, 777w, 768s, 731m, 722m, 705w, 668m, 653w, 644w, 604m, 542w, 497w, 467w. ^{1}H NMR ($CDCl_3$): δ = 7.30 -7.21 (3x m, 8H, aryl*H*), 6.75 (s, 4H, aryl*H*), 6.34 (s, 2H, C*H*), 5.64 (s, 4H, 2x CH_2Cl_2), 1.69 (s, 18H, OC(CH_3)$_3$), 1.43 (s, 36H, C(CH_3)$_3$), 1.22 (s, 36H, C(CH_3)$_3$). ^{51}V NMR ($CDCl_3$) δ = -467.9 ($w_{1/2}$ = 528 Hz). Single crystals of **2**.2MeCN were grown from a saturated acetonitrile solution on prolonged standing at 0 ^{o}C.

Synthesis of {$\mathbf{L^2}$[VO(O*n*Pr)(THF)]$_2$} (**3**)

As for **1**, but using α,α,α′,α′-tetrakis(3,5-di-*tert*-butyl-2-hydroxyphenyl)-*m*-xylene ($\mathbf{L^2}H_4$, 4.1 g, 4.4 mmol) and vanadium oxytri-*n*-propoxide (1.0 mL, 4.5 mmol). Crystallization using THF/light petroleum afforded orange needles of **3** (2.0 g, 35 %). MS (E.I.): 1170.6 $[M\text{-}2THF]^+$, 1110.5 $[M\text{-}HO\mathit{n}Pr\text{-}2THF]^+$. IR (Nujol, KBr, cm^{-1}): 1595m, 1406m, 1361s, 1217s, 1154m, 1118s, 1104s, 1030s, 992s, 910w, 882w, 846s, 787s, 720s, 695w, 649s, 601m, 499w, 449w. Found: C, 71.60; H, 8.41. $C_{70}H_{100}O_8V_2$ (sample dried *in vacuo* for 24 h leads to loss of THF x2) requires C, 71.76; H, 8.60 %. ^{1}H NMR ($CDCl_3$): δ = 7.18 (d, 4H, *J* = 2.35, aryl*H*), 7.15 (d, 4H, *J* = 2.35, aryl*H*), 7.10 (s, 1H, aryl*H*), 7.02 (t, 1H, *J* = 7.83, aryl*H*), 6.80 (d, 2H, *J* = 7.93, aryl*H*), 6.25 (s, 2H, Ar_3-C*H*), 5.34 (t, 4H, *J* = 6.53, OCH_2CH_2), 3.74 (bm, 8H, THF α-*H*), 1.98 (sextet, 4H, *J* = 7.00, $CH_2CH_2CH_3$), 1.86 (bm, 8H, THF β-*H*), 1.42 (s, 36H, *t*Bu), 1.17 (s, 36H, *t*Bu), 1.09 (t, 6H, J = 7.35, CH_2CH_3). ^{51}V NMR ($CDCl_3$) δ = -432.5 ($w_{1/2}$ =170 Hz).

Synthesis of {[VO(*t*BuO)][V(N*p*-MeC_6H_4)(*t*BuO)](μ-*p*-L^1)}·CH_2Cl_2 (**4**·CH_2Cl_2)

[V(N*p*-MeC_6H_4(O*t*Bu)$_3$] (3.3 g, 8.8 mmol) and L^1H_4 (4.1 g, 4.4 mmol) were refluxed in toluene (30 mL) for 12 h. On cooling, the volatiles were removed *in-vacuo*, and the residue was extracted into either acetonitrile (30 ml) or dichloromethane (30 ml). Cooling to -20 ^{o}C afforded **4** as small yellow/orange crystals. Yield 2.05 g, 34 %. $C_{79}H_{111}NO_7V_2\cdot 2CH_2Cl_2$ requires C 66.70, H 7.95, N, 0.96 %. Found C 66.22, H 8.32, N, 1.02 %. MS (solvated with CH_2Cl_2 and diluted with MeCN for positive nano-electrospray technique): *m/z* 1291 $[M]^+$, 1185 $[M\text{-}H_2N\mathit{p}\text{-}C_6H_4]^+$. IR: 1593w, 1568w, 1508w, 1403m, 1362s, 1291m, 1261s, 1238w, 1224m, 1201w, 1153m, 1115m, 1104s, 1018s, 974s, 912w, 876m, 844m, 800s, 778m, 769m, 737m, 705w, 669w, 644w, 603w,

573w, 542w, 468w. ^{1}H NMR ($CDCl_3$): δ = 7.22 - 7.13 (3x m, 12H, aryl*H*), 6.68 (s, 4H, aryl*H*), 6.27 (s, 2H, C*H*), 5.22 (s, 2H, CH_2Cl_2), 2.23 (s, 3H, tolylCH_3), 1.93 (s, 3H, CH_3CN), 1.69 (s, 18H, OC(CH_3)$_3$), 1.44 (overlapping s, 27H, C(CH_3)$_3$), 1.36 (s, 9H, C(CH_3)$_3$), 1.23 (overlapping s, 27H, C(CH_3)$_3$), 1.15 (s, 9H, C(CH_3)$_3$); ^{51}V NMR ($CDCl_3$) δ = -468.2 ($w_{1/2}$ = 277 Hz), -558.5 ($w_{1/2}$ = 297 Hz).

Synthesis of {[VO(*t*BuO)][V(N*p*-$CF_3C_6H_4$)(*t*BuO)](μ-*p*-L^1)}·CH_2Cl_2 (**5**·CH_2Cl_2)

As for **7**, but using [V(N*p*-$CF_3C_6H_4$(O*t*Bu)$_3$] (3.8 g, 8.8 mmol) and L^1H_4 (4.1 g, 4.4 mmol) affording on cooling (-20 ^{o}C) **5** as pale yellow/orange needles (yield 2.57 g, 41 %). $C_{79}H_{106}F_3NO_7V_2$·CH_2Cl_2 requires C, 67.40, H, 7.64, N, 0.98 %. Found C 67.33, H 7.77, N 0.89 %. MS (solvated with CH_2Cl_2 and diluted with MeCN for positive nano-electrospray technique): *m/z* 1342 $[MH]^+$, 1269 [MH-O*t*Bu]. IR: 1623w, 1599w, 1526w, 1507w, 1402m, 1375s, 1362s, 1327s, 1320s, 1292m, 1259s, 1237m, 1213m, 1200m, 1152s, 1117s, 1104s, 1066s, 976s, 911m, 873m, 841s, 801s, 768s, 755w, 735w, 720w, 705w, 696w, 667m, 652w, 643w, 621w, 597m, 573w, 540w, 503w, 494w. ^{1}H NMR ($CDCl_3$): δ = 7.33 - 7.13 (3x m, 8H, aryl*H*), 6.68 (s, 4H, aryl*H*), 6.27 (s, 2H, C*H*), 5.22 (s, 2H, CH_2Cl_2), 1.93 (s, 3H, CH_3CN), 1.69 (s, 18H, OC(CH_3)$_3$), 1.53 (s, 9H, C(CH_3)$_3$), 1.37 (s, 27H, C(CH_3)$_3$), 1.23 (s, 9H, C(CH_3)$_3$), 1.17 (s, 27H, C(CH_3)$_3$); ^{19}F NMR ($CDCl_3$) δ = -61.2; ^{51}V NMR ($CDCl_3$) δ = -467.7 ($w_{1/2}$ = 520 Hz), -539.6 ($w_{1/2}$ = 296 Hz).

Synthesis of {[V(THF)(N*p*-MeC_6H_4)Cl]$_2$(μ-*p*-L^1)} **6**·4toluene

L^1H_4 (1.00 g, 1.08 mmol) and Na (0.10 g, 4.35 mmol) were stirred in THF (30 ml) at ambient temperature for 12 h. The solution was then cooled to -78 ^oC and solid [V(N*p*-MeC_6H_4)Cl_3] (0.60 g, 2.29 mmol) was added. The mixture was allowed to warm to room temperature and was stirred for 12 h. Volatiles were removed *in-vacuo*, and the residue was extracted into toluene (30 ml) or dichloromethane (30 ml). Brown/red prisms of **6** were formed on prolonged standing (1 - 2 days) at 0 ^oC. Yield: 1.61 g, 83 %. $C_{87}H_{102}Cl_2N_2O_6V_2$ (sample crystallized from CH_2Cl_2, **6**·CH_2Cl_2) requires C, 68.95, H, 6.78, N, 1.84 %. Found C 69.92*, H 7.16, N 2.05 %. * Despite repeated attempts, we were unable to obtain closer %C values. MS (EI, positive mode): *m/z* 1527 (M^+ – Cl – THF), 1459 (M^+ – 2Cl – tolylNH_2). IR: 3544w, 1597w, 1568m, 1506w, 1291m, 1261s, 1240m, 1224m, 1201w, 1153w, 1118m, 1104m, 1007s, 968s, 912w, 876m, 844m, 799m, 778w, 768m, 722s, 668w, 643w, 603w, 496w, 462w. ^{1}H NMR ($CDCl_3$): δ = 7.45 – 6.92 (3x m, 17H, aryl*H* including one toluene), 6.56 (s, 2H, C*H*), 6.49 (d, J 8.0 Hz, 4H, aryl*H*), 5.97 (d, J 8.0 Hz, 4H, aryl*H*), 4.29 (m, 8H, THF α-H), 2.37 (s, 6H. C$H_3C_6H_4$), 2.17 (s, 3H, CH_3 of toluene), 2.02 (m, 8H, THF β-H), 1.31 (s, 36H, C(CH_3)$_3$), 1.23 (s, 36H, C(CH_3)$_3$); ^{51}V NMR ($CDCl_3$) δ = -7.3 ($w_{1/2}$ = 3373 Hz).

Synthesis of {[V(THF)(N*p*-$CF_3C_6H_4$)Cl]$_2$(μ-*p*-L^1)} **7**

As for **8**, but using [V(N*p*-$CF_3C_6H_4$)Cl_3] (0.72 g, 2.28 mmol) and L^1H_4 (1.00 g, 1.08 mmol) and Et_3N (0.63 ml, 4.55 mmol) affording red/brown **7**; the complex can be recrystallized from cold toluene or dichloromethane, yield 0.71 g, 47 %. $C_{114}H_{126}Cl_2F_6N_2O_6V_2$ ·CH_2Cl_2 requires C, 63.73, H, 6.89, N, 1.71 %. Found C 63.56, H 7.20, N 1.47 %. MS (EI, positive mode) 1411.5 [MH –

2THF]$^+$, 1340.6 [MH – 2THF – 2Cl]$^+$, 1250 [MH – 2THF – $H_2NC_6H_4CF_3$]$^+$, 1089 [MH – 2THF – $2H_2NC_6H_4CF_3$]$^+$. IR: 2335w, 1693w, 1651w, 1616w, 1600w, 1507w, 1406m, 1364s, 1321s, 1261s, 1240w, 1226m, 1201w, 1168s, 1122s, 1104s, 1066s, 1021s, 956w, 910w, 873m, 841s, 803s, 773m, 753w, 728s, 692m, 668w, 645w, 626w, 596m, 556w, 502w, 464w. ^{1}H NMR ($CDCl_3$): δ = 7.54 – 7.02 (3x m, 16H, aryl*H* + imidoaryl*H*), 6.76 (s, 4H, aryl*H*), 6.35 (s, 2H, C*H*), 5.29 (s, 2H, CH_2Cl_2), 3.12 (bm, 8H, THF α-*H*), 1.85 (bm, 8H, THF β-*H*), 1.43 (s, 36H, C(CH_3)$_3$), 1.23 (s, 36H, C(CH_3)$_3$); ^{19}F NMR ($CDCl_3$) δ = -60.7; ^{51}V NMR (C_6D_6) δ = -211.1 ($w_{1/2}$ = 647 Hz).

Synthesis of {**L**^{3}(VO)$_2$(μ-O*n*Pr)$_2$} (**8**)

2-(α-(2-Hydroxy-3,5-di-*tert*-butylphenyl)benzyl)-4,6-di-*tert*-butylphenol (**L**^{3}H$_2$, 4.1 g, 8.2 mmol) was dissolved in tetrahydrofuran (40 mL). Vanadium oxytri-*n*-propoxide (1.9 mL, 8.4 mmol) was added via syringe and the solution was stirred at room temperature for 16 h. The volatiles were removed *in vacuo*, following which crystallization using warm light petroleum gave red needles of the vanadium dimer **8** (3.6 g, 70 %). MS (EI, *m/z*): 624.4 [M]$^+$, 564.4 [M-O*n*Pr]. IR (Nujol, KBr, cm^{-1}): 1599m, 1381m, 1289w, 1220s, 1153s, 1103s, 1060s, 989s, 911w, 875w, 855m, 836s, 800m, 770m, 745m, 705m, 652s, 599m, 503w, 451w. Found: C, 72.82; H, 8.39. $C_{76}H_{106}O_8V_2$ requires C, 73.05; H, 8.55 %. ^{1}H NMR ($CDCl_3$): δ = 7.33 (d, 4H, *J* = 2.30, aryl*H*), 7.27 d, (4H, *J* = 2.30, aryl*H*), 7.21-7.15 (m, 4H, aryl*H*), 7.00 (d, 4H, *J* = 7.95, aryl*H*), 6.38 (s, 2H, Ar$_3$C*H*), 5.37 (t, 4H, *J* = 6.03, OCH_2CH$_2$), 1.99 (sextet, 4H, CH$_2$CH_2CH$_3$), 1.47 (s, 36H, *t*Bu), 1.26 (s, 36H, *t*Bu), 1.10 (t, 6H, *J* = 7.40, CH$_2$CH$_3$). ^{51}V NMR ($CDCl_3$): δ = -433.6 ($w_{1/2}$ = 170 Hz).

Polymer Characterization

The melt transition temperatures (T_m) of the polyethylene (PE) and ethylene/propylene copolymer (EPR) were determined by differential scanning calorimetry (DSC) with a Shimadzu DSC-60 instrument. The polymer samples were heated at 50 ^oC/min from 20 ^oC to 200 ^oC, held at 200 ^oC for 5 min, and cooled to 0 ^oC at 20 ^oC/min. The samples were held at this temperature for 5 min, and then reheated to 200 ^oC at 10 ^oC/min. The reported T_m was determined from the second heating scan unless otherwise noted.

Molecular weights (M_w and M_n) and molecular weight distributions (MWDs) of PE and EPR were determined using a Waters GPC2000 gel permeation chromatograph equipped with four TSKgel columns (two sets of TSKgelGMH$_6$-HT and two sets of TSKgelGMH$_6$-HTL) at 140 ^oC using polyethylene calibration. *o*-Dichlorobenzene (ODCB) was used as the solvent.

Polymerization Procedure: Polymerization reactions were performed in a parallel pressure reactor (Argonaut Endeavor® Catalyst Screening System) containing 8 reaction vessels (15 mL) each equipped with a mechanical stirrer and monomer feed lines. At first, a toluene solution (and a toluene solution of ETA where necessary) were injected into each vessel. *For ethylene polymerization*, the solution was heated to the polymerization temperature (T_p) and thermally equilibrated, and the nitrogen atmosphere was replaced with ethylene and the solution was saturated with ethylene at the polymerization pressure. *For ethylene/propylene copolymerization*, the solution was heated to the T_p and thermally equilibrated, and the nitrogen atmosphere was replaced with propylene and the reaction vessels were pressurized with propylene (0.4 MPa at 25 ^oC), then ethylene was introduced into the reactor up to the polymerization pressure. *In all cases*

the polymerization was started by addition of a toluene solution of alkyl aluminum or alkyl aluminum chloride followed by addition of a toluene solution of the vanadium complex (0.50 mL toluene solution of complex followed by 0.25 mL toluene wash). The total volume of the reaction mixture was 5 mL for all polymerizations. The pressure was kept constant by feeding ethylene on demand. After the reaction, the polymerization was stopped by addition of excess isobutyl alcohol. The resulting mixture was added to acidified methanol (45 ml containing 0.5 ml of concentrated HCl). The polymer was recovered by filtration, washed with methanol (2 × 10 ml) and dried in a vacuum oven at 80 ^{o}C for 10 h.

Crystallography: Single crystal X-ray diffraction data for **7**.toluene.thf were collected in series of ω-scans using a Stoe IPSD2 image plate diffractometer utilising monochromated Mo radiation (λ = 0.71073 Å). Standard procedures were employed for the integration and processing of the data using X-RED. [25] Samples were coated in a thin film of perfluoropolyether oil and mounted at the tip of a glass fibre located on a goniometer. Data were collected from crystals held at 150 K in an Oxford Cryosystems nitrogen gas cryostream.

All other single crystal data were collected using series of ω-scans by the EPSRC UK National Crystallography Service; data for **3** was collected at the Diamond Light Source (I19, synchrotron radiation λ = 0.6889 Å); data for the remaining samples were collected using a radiation from a Mo rotating anode source. Samples were mounted using MiTeGen loops and held at 100 K in an Oxford Cryosystems nitrogen gas cryostream. Data were corrected for Lp effects and for absorption. CrystalClear-SM Expert 3.1 b27 (Rigaku, 2012); cell refinement: CrystalClear-SM Expert 3.1 b27 (Rigaku, 2012); data reduction: CrystalClear-SM Expert 3.1 b27 (Rigaku, 2012);

program(s) used to solve structure: SHELXS97 [26]; program(s) used to refine structure: SHELXL2013 [27]

Many of the structures contained small-scale disorder involving the t-butyl groups. This was handled using standard procedures. The SQUEEZE [28] routine was applied to model scattering from regions of disordered solvent in these structures: **3** and **8**. The crystal examined for **6**·MeCN was found to be twinned and this was handled by routine techniques and the final model refined using the HKLF5 formalism using all observed data.

CCDC 1404522-3, 1404527-8 and 1404530-2 (structures **1** & **3**, **4** & **5, 6** – **8**) and 1048777 (structure **2**) contain the supplementary crystallographic data for this paper. These data can be obtained free of charge from The Cambridge Crystallographic Data Centre via www.ccdc.cam.ac.uk/data_request/cif.

Acknowledgements: The EPSRC Mass Spectrometry Service (Swansea, UK) and the EPSRC National X-ray Crystallographic Service (Southampton) are thanked for data collection. CR thanks the EPSRC for an Overseas Travel grant.

Supporting Information Available: X-ray crystallographic files CIF format for the structure determinations of compounds **1**·2THF, **2**·2MeCN, **3**, **4**·CH_2Cl_2, **5**·CH_2Cl_2, **6**·4toluene, **7** and **8**.

Table 6. Crystallographic data for the complexes **1**·2THF, **2**·2MeCN and **3**.

Compound	**1**·2(THF)	**2**·2MeCN	**3**
Formula	$C_{78}H_{116}V_2O_{10}\cdot 2C_4H_8O$	$C_{72}H_{104}V_2O_8\cdot 2CH_3CN$	$C_{78}H_{116}V_2O_{10}$

Formula weight	1459.80	1281.53	1315.66
Crystal system	orthorhombic	triclinic	monoclinic
Space group	Pbca	$P\bar{1}$	$P2/n$
Unit cell dimensions			
a (Å)	23.8164(16)	9.1413(7)	20.18(2)
b (Å)	18.9585(7)	11.0130(8)	15.820(16)
c (Å)	18.6002(6)	18.8731(13)	26.50(3)
α (º)	90	74.468(8)	90
β (º)	90	89.494(9)	110.686(11)
γ (º)	90	85.010(9)	90
V (Å^3)	8398.4(7)	1823.5(20	7915(14)
Z	4	1	4
Temperature (K)	100(2)	100(2)	100(2)
Wavelength (Å)	0.71075	0.71075	0.71075
Calculated density (g.cm^{-3})	1.155	1.167	1.021
Absorption coefficient (mm^{-1})	0.279	0.309	0.264
Transmission factors (min./max.)	0.9753 and 0.9917	0.642 and 1.000	0.355 and 1.000
Crystal size (mm^3)	0.09 × 0.08 × 0.03	0.06 × 0.05 × 0.01	0.04 × 0.04 × 0.01
θ(max) (°)	27.46	25.601	18.06
Reflections measured	57655	28762	30414
Unique reflections	9280	6855	6040
R_{int}	0.1195	0.0975	0.2574
Reflections with $F^2 > 2\sigma(F^2)$	5352	3107	3038
Number of	464	388	578

parameters			
R_1 [$F^2 > 2\sigma(F^2)$]	0.0484	0.1541	0.2176
wR_2 (all data)	0.1110	0.4724	0.5275
GOOF, S	0.913	1.431	1.522
Largest difference peak and hole (e Å^{-3})	0.346 and –0.454	0.514 and –0.871	0.777 and –0.463

Table 6 con't. Crystallographic data for the complexes **4**·CH_2Cl_2 and **5**·CH_2Cl_2

Compound	**4**·CH_2Cl_2	**5**·CH_2Cl_2
Formula	$C_{79}H_{111}NV_2O_7 \cdot CH_2Cl_2$	$C_{79}H_{106}NF_3V_2O_7 \cdot CH_2Cl_2$
Formula weight	1373.49	1425.45
Crystal system	triclinic	triclinic
Space group	$P\bar{1}$	$P\bar{1}$
Unit cell dimensions		
a (Å)	9.4460(6)	9.413(7)
b (Å)	11.1800(7)	11.244(8)
c (Å)	19.3754(13)	19.369(13)
α (º)	77.635(4)	79.20(4)
β (º)	81.522(4)	80.90(3)
γ (º)	85.307(5)	84.40(4)
V (Å^3)	1974.2(2)	1983(2)
Z	1	1
Temperature (K)	100(2)	100(2)
Wavelength (Å)	0.71075	0.71073
Calculated density (g.cm^{-3})	1.155	1.193
Absorption coefficient (mm^{-1})	0.354	0.36

Transmission factors (min./max.)	0.479 and 1.000	0.796 and 1.000
Crystal size (mm^3)	0.04 x 0.03 x 0.01	0.07 x 0.04 x 0.02
θ(max) (°)	25.0	22.5
Reflections measured	21387	17204
Unique reflections	6954	5167
R_{int}	0.1230	0.072
Reflections with $F^2 > 2\sigma(F^2)$	2929	3631
Number of parameters	477	527
R_1 [$F^2 > 2\sigma(F^2)$]	0.0896	0.105
wR_2 (all data)	0.2555	0.282
GOOF, S	0.968	1.11
Largest difference peak and hole (e $Å^{-3}$)	0.399 and -0.398	0.55 and -0.754

Table 6 con't. Crystallographic data for the complexes **6**·4toluene, **7** and **8**

Compound	**6**·4toluene	**7**	**8**
Formula	$C_{114}H_{132}N_2Cl_2V_2O_6{\cdot}4C_7H_8$	$C_{86}H_{110}N_2Cl_2F_6V_2O_6$	$C_{76}H_{106}V_2O_8$
Formula weight	1798.99	1554.53	1249.49
Crystal system	triclinic	triclinic	triclinic
Space group	$P\bar{1}$	$P\bar{1}$	$P\bar{1}$
Unit cell dimensions			
a (Å)	10.8048(12)	10.5705(7)	11.3476(8)
b (Å)	14.4744(13)	11.3001(8)	12.2819(19)
c (Å)	18.3207(19)	17.4045(11)	16.8097(11)

α (º)	74.937(8)	94.986(7)	100.861(4)
β (º)	84.606(9)	90.688(7)	99.097(4)
γ (º)	69.796(8)	93.257(7)	108.087(5)
V (Å^3)	2596.5(5)	2067.4(2)	2127.4(3)
Z	1	1	1
Temperature (K)	150(2)	100(2)	100(2)
Wavelength (Å)	0.71073	0.71075	0.71073
Calculated density (g.cm^{-3})	1.151	1.249	0.975
Absorption coefficient (mm^{-1})	0.284	0.356	0.263
Transmission factors (min./max.)	0.786 and 0.818	0.688 and 1.00	0.9818 and 0.9921
Crystal size (mm^3)	0.40 x 0.25 x 0.20	0.07 x 0.06 x 0.01	0.07 × 0.06 × 0.03
θ(max) (°)	25.328	27.486	27.49
Reflections measured	18331	25769	9683
Unique reflections	9342	9232	9683
R_{int}	0.0776	0.0763	0.059
Reflections with $F^2 > 2\sigma(F^2)$	3813	5672	6948
Number of parameters	525	469	392
R_1 [$F^2 > 2\sigma(F^2)$]	0.0652	0.0942	0.0566
wR_2 (all data)	0.1661	0.2885	0.1587
GOOF, S	0.785	1.037	1.057
Largest difference peak and hole (e Å^{-3})	0.510 and -0.303	1.376 and -0.568	0.631 and –0.502

References

[1] (a) R. Galletti and G. Pampaloni, *Coord. Chem. Rev.* **2010**, *254*, 525-536. (b) K. Nomura and W. Zhang, *Chem Sci*. **2010**, *1*, 161-173. (c) Y. R. Patil in: *Olefins Polymerization Reactivity of Niobium-Based Metal Complexes*, US, Lambert Academic Publishing, **2011**. (c) D. Wang, Z. Zhao, T. B. Mikenas, X. Lang, L. G. Echevskaya, C. Zhao, M. A. Matsko and W. Wu, *Polym. Chem*. **2012**, *3*, 2377-2382.

[2] See for example (a) H. Hagen, J. Boersma and G. van Koten, *Chem. Soc. Rev*. **2002**, *31*, 357-364. (b) S. Gambarotta, *Coord. Chem. Rev*. **2003**, *237*, 229-243. (c) Y. Onishi, S. Katao, M. Fujiki and K. Nomura, *Organometallics* **2008**, *27*, 2590-2596. (d) J.Q. Wu, L. Pan, N. H. Hu and Y. S. Li, *Organometallics* **2008**, ***27***, 3840-3848. (e) C. Redshaw, *Dalton Trans*. **2010**, *39*, 5595-5604 and references therein.

[3] (a) D. Takeuchi, *Dalton Trans.* **2010**, *39*, 311-328. (b) K. Nomura and W. Zhang, *Chem. Rev.* **2011**, *111*, 2342-2362. (c) J. -Q. Wu and Y. -S. Li, *Coord. Chem. Rev*. **2011**, *255*, 2303-2314. (d) S. W. Zhang, L. -P. Lu, B. -X. Li and Y. -S. Li, *J. Polym. Sci. A, Polym. Chem.* **2012**, *50*, 4721-4731. (e) S. W. Zhang, L. -P. Lu, Y. -Y. Long and Y. -S. Li, *J. Polym. Sci. A, Polym. Chem*. **2013**, *51*, 844-854. (f) L. –P. Lu, J. –B. Wang, J. –Y. Liu and Y. –S. Li, *J. Polym. Sci. A, Polym. Chem*. **2014**, *52*, 2633-2642.

[4] (a) C. Redshaw, L. Warford, S. H. Dale and M. R. J. Elsegood, *Chem. Comm.* **2004**, 1954-1956. (b) C. Redshaw, M. A. Rowan, D. M. Homden, S. H. Dale, M. R. J. Elsegood, S. Matsui and S. Matsuura, *Chem. Comm*. **2006**, 3329-3331. (c) C. Redshaw, M. A. Rowan, L. Warford, D. M. Homden, A. Arbaoui, M. R. J. Elsegood, S. H. Dale, T. Yamato, C. P. Casas and S. Matsui, *Chem. Eur. J.* **2007**, *13*, 1090-1107. (d) D. M. Homden, C. Redshaw, L. Warford, D. L. Hughes, J. A. Wright, S. H. Dale and M. R. J. Elsegood, *Dalton Trans*. **2009**, 8900-8910. (e) C. Redshaw, D. M. Homden, D. L. Hughes, J. A. Wright and M. R. J. Elsegood, *Dalton Trans*. **2009**, 1231-1242. (f) L. Clowes, C. Redshaw and D. L. Hughes, *Inorg. Chem*. **2011**, *50*, 7838-7845. (g) C. Redshaw, L. Clowes, D. L. Hughes, M. R. J. Elsegood and T. Yamato, *Organometallics* **2011**, *30*, 5620-5624. (h) C. Redshaw, M. J. Walton, D. S. Lee, C. Jiang, M. R. J. Elsegood and K. Michiue, *Chem. Eur. J.* **2015**, *21*, 5199-5210. (i) C. Redshaw, M. J. Walton, K. Michiue, Y.

Chao, A. Walton, P. Elo, V. Sumerin, C. Jiang and M. R. J. Elsegood, *Dalton Trans*. **2015**, *44*, 12292-12303.

[5] L.H. Tang, E. P. Wasserman, D. R. Neithamer, R. D. Krystosek, Y. Cheng, P. C. Price, Y. Y. He and T. J. Emge, *Macromolecules* **2008**, *41*, 7306-7315.

[6] J. Zhang, C. Jian, Y. Gao, L. Wang, N. Tang and J. Wu, *Inorg. Chem*. **2012**, *51*, 13380-13389.

[7] Y. Al-Khafaji, X. Sun, T. J. Prior, M. R. J. Elsegood and C. Redshaw, *Dalton Trans*. **2015**, *44*, 12349-12356.

[8] A.G. Fisch, J. N. da Silveira, N. S. M. Cardozo, A. R. Secchi, J. H. Z. dos Santos and J. B. P. Soares, *J. Mol. Cat A Chem*. **2013**, *366*, 74-83.

[9] R. E. LaPointe, J. C. Stevens, P. N. Nickias and M. H. McAdon, Dow Chemicals USA, EP 0 520 732 B1, 1992.

[10] (a) R. Figueroa, R. D. Froese, Y. He, J. Klosin, C. N. Theriault and K. A. Abboud, *Organometallics* **2011**, *30*, 1695-1709. (b) P. P. Fontaine, R. Figueroa, S. D. McCann, D. Mort and J. Klosin, *Organometallics* **2013**, *32*, 2963-2972. (c) T. R. Boussie, G. M. Diamond, C. Goh, K. A. Hall, A. M. LaPointe, M. K. Leclerc, V. Murphy, J. A. W. Shoemaker, H. Turner, R. K. Rosen, J. C. Stevens, F. Alfano, V. Busico, R. Cipullo and G. Talarico, *Angew. Chem. Int. Ed*. **2006**, *45*, 3278-3283. (d) P. S. Chum and K. W. Swogger, *Prog. Polym. Sci*. **2008**, *33*, 797-819. (e) For a recent review on the use of Post-Metallocenes catalysts for industrial polyolefin production, see M. C. Baier, M. A. Zuideveld and S. Mecking, *Angew. Chem. Int. Ed*. **2014**, *53*, 9722-9744.

[11] (a) N. Desmangles, S. Gambarotta, C. Bensimon, S. Davis and H. Zahalka, *J. Organomet, Chem*. **1998**, *562*, 53-60. (b) Y. Ma, D. Reardon, S. Gambarotta and G. Yap, *Organometallics* **1999**, *18*, 2773. (c) H. Hagen, J. Boersma, M. Lutz, A. L. Spek and G. van Koten, *Eur. J. Inorg. Chem*. **2001**, 117. (d) M. Arndt-Rosenau, M. Hoch, J. Sundermeyer, J. Kipke and X. Li, *US Pat*. 01 304551, **2003**. (e) Y. Nakayama, H. Bando, Y. Sonobe and T. Fujita, *J. Mol. Catal. A: Chem*. **2004**, *213*, 141. (f) S. Cuomo, S. Milione and A. Grassi, *J. Polym, Sci., Part A: Polym. Chem*. **2006**, *44*, 3279. (g) S. Zhang, W. -C. Zhang, D.-D. Shang, Z. -Q. Zhang, and Y. -X. Wu, *Dalton Trans*. **2015**, DOI 10.1039/c5dt00675a

[12] See for example (a) C. R. Randall and W. H. Armstrong, *J. Chem. Soc., Chem. Commun*. **1988**, 986-987. (b) G. Asgedom, A. Sreedhara, J. Kivikoski, E. Kolehmainen and C. P. Rao, *J. Chem. Soc., Dalton Trans*. **1996**, 93-97.

[13] (a) M. Mazzanti, C. Floriani, A. Chiese-Villa and C. Guastini, *J. Chem. Soc., Dalton Trans*. **1989**, 1793-1798. (b) P. J. Toscano, E. J. Schermerhorn, C. Dettelbacher, D. Macherone and J. Zubieta, *J. Chem. Soc., Chem. Comm*. **1991**, 933-934.

[14] (a) W. Clegg, M. R. J. Elsegood, S. J. Teat, C. Redshaw and V. C. Gibson, *J. Chem. Soc., Dalton Trans*. **1998**, 3037-3040. (b) W. Clegg, *J. Chem. Soc., Dalton Trans*. **2000**, 3223-3232.

[15] (a) C. Redshaw in Olefin Upgrading Catalysis by Nitrogen-based Metal Complexes I, Eds. G. Giambastini and J. Cámpora, Springer **2011**. (b) S. Zhang and K. Nomura, *Catal Surv Asia* **2011**, *15*, 127-133.

[16] (a) E. A. Maatta, *Inorg. Chem*. **1984**, *23*, 2561-2562. (b) D. D. Devore, J. D. Lichtenhan, F. Takusagawa and E. A. Maatta, *J. Am. Chem. Soc*. **1987**, *109*, 7408-7416.

[17] F. H. Allen, *Acta Crystallogr. Sect. B: Struct. Sci*., **2002**, *58*, 380-388.

[18] Spiro compounds related to motif **I** in the CSD: (a) A. M. Litwak, F. Grynazpan, O. Aleksiuk, S. Cohen and S. E. Biali, *J. Org. Chem*. **1983**, *58*, 393-402. (b) F. Grynszpan and S. E. Biali, *J. Chem. Soc., Chem. Commun*. **1994**, 2545-2546. (c) O. Aleksiuk, S. Cohen and S. E. Biali, *J. Am. Chem. Soc*.**1995**, *117*, 9645-9652. (d) F. Grynszpan and S. E. Biali, *J. Org. Chem*. **1996**, *61*, 9512-9521. (e) J. Wöhnert, J. Brenn, M. Stoldt, O. Aleksiuk, F. Grynszpan, I. Thondorf and S. E. Biali, *J. Org. Chem*. **1998**, *63*, 3866-3874. (f) K. Agharia, O. Aleksiuk, S. E. Biali, V. Böhmer, M. Frings and I. Thondorf, *J. Org. Chem*. **2001**, *66*, 2891-2899. (g) K. Agharia and S. E. Biali, *J. Am. Chem. Soc*. **2001**, *123*, 12495-12503.

[19] A. G. Maestri and S. N. Brown, *Inorg. Chem*. **2004**, *43*, 6996-7004.

[20] For early use of ETA, see (a) A. Gumboldt, J. Helberg and G. Schleitzer, *Makromol. Chem*. **1967**, *101*, 229-245. (b) D. L. Christman, *J. Polym. Sci. Part A*, **1972**, *10*, 471-487. (c) E. Addison, A. Deffieux, M. Fontanille and K. Bujadoux, *J. Polym. Sci, Part A*, **1994**, *32*, 1033-1041.

[21] E. W. Hansen, R. Blom and O. M. Bade, *Polymer* **1997**, *38*, 4295-4304.

[22] W. Wang and K. Nomura, *Macromolecules*, **2005**, *38*, 5905-5913.

[23] E. Mùller, A. Schick and R. Mayer, *Chem. Ber*. **1960**, *93*, 2649-2662.

[24] APCI refers to the ionization method, Atmospheric Pressure Chemical Ionization, in which samples introduced into the APCI source via an Atmospheric Solids Analysis Probe (ASAP) are vaporized then ionized using a corona discharge (~ 4µA). The benefit of using ASAP is that samples can be introduced at ambient temperature as solids or in solution, then the temperature in the source is increased until the sample vaporizes.

[25] X-AREA v 1.64, STOE & Cie GmbH, Darmstadt, **2012**.

[26] G. Sheldrick, *Acta Crystallogr. Sect. A: Found. Crystallogr*. **2008**, *64*, 112-122.

[27] A. L. Spek, *Acta Cryst*. **2009**, *D65*, 148-155.

[28] A. L. Spek, *Acta Crystallogr*. **1990**, A46, C34.